National Park Service
U.S. Department of the Interior

Natural Resource Program Center

Monitoring of Retrogressive Thaw Slumps in the Arctic Network, 2010 Baseline Data

Three-dimensional Modeling with Small-format Aerial Photographs

Natural Resource Data Series NPS/ARCN/NRDS—2010/123

ON THE COVER
Main scarp region of a retrogressive thaw slump in Noatqak National Preserve (slump NOAT172) on 21 June 2010. Shiny near-vertical faces on the left and in the center are large Pleistocene ice wedges.

Monitoring of Retrogressive Thaw Slumps in the Arctic Network, 2010 Baseline Data

Three-dimensional Modeling with Small-format Aerial Photographs

Natural Resource Data Series NPS/ARCN/NRDS—2010/123

David K. Swanson and Ken Hill

National Park Service
Fairbanks Administrative Center
4175 Geist Rd.
Fairbanks, AK 99709

December 2010

U.S. Department of the Interior
National Park Service
Natural Resource Program Center
Fort Collins, Colorado

The National Park Service, Natural Resource Program Center publishes a range of reports that address natural resource topics of interest and applicability to a broad audience in the National Park Service and others in natural resource management, including scientists, conservation and environmental constituencies, and the public.

The Natural Resource Data Series is intended for timely release of basic data sets and data summaries. Care has been taken to assure accuracy of raw data values, but a thorough analysis and interpretation of the data has not been completed. Consequently, the initial analyses of data in this report are provisional and subject to change.

All manuscripts in the series receive the appropriate level of peer review to ensure that the information is scientifically credible, technically accurate, appropriately written for the intended audience, and designed and published in a professional manner.

This report received informal peer review by subject-matter experts who were not directly involved in the collection, analysis, or reporting of the data.

Views, statements, findings, conclusions, recommendations, and data in this report do not necessarily reflect views and policies of the National Park Service, U.S. Department of the Interior. Mention of trade names or commercial products does not constitute endorsement or recommendation for use by the U.S. Government.

This report is available from the National Park Service, Arctic Inventory and Monitoring Network (http://science.nature.nps.gov/im/units/arcn/) and the Natural Resource Publications Management website (http://www.nature.nps.gov/publications/NRPM).

Please cite this publication as:

Swanson, D. K. and K. Hill. 2010. Monitoring of retrogressive thaw slumps in the Arctic Network, 2010 baseline data: Three-dimensional modeling with small-format aerial photographs. Natural Resource Data Series NPS/ARCN/NRDS—2010/123. National Park Service, Fort Collins, Colorado.

NPS 953/106254, December 2010

Contents

Figures

Tables

Page

Abstract

Retrogressive thaw slumps (RTS) are caused by thaw of massive ground ice on slopes and combine subsidence, mass movement, and water erosion. They can expose several hectares of bare soil that is susceptible to erosion into nearby water bodies. In the summer of 2010, oblique aerial-photographs of 24 selected RTS in Noatak National Preserve (NOAT) and Gates of the Arctic National Park and Preserve (GAAR) were taken with a hand-held, 35-mm digital camera. This photography was used to create high-resolution three-dimensional topographic models with photographic overlay. Accurate ground control was obtained at 14 of the slumps by surveying the location of temporary targets that were captured on the aerial photographs and then removed; this allowed us to scale the models and obtain measurements of elevation, area, and volume. Ground control will be obtained at the remaining slumps in future years. These 3D models are the baseline that will be used with models created in the future from new photographs to track the rate of growth or stabilization of the slumps, the volume of material displaced, and the rate of revegetation.

The study slumps ranged in size from less than 1 ha to over 4 ha and were generally oval shaped with a steep main scarp 2 to 10 m high along the uphill side. Most of the slumps exposed ground ice that was actively melting, causing material to fall from the main scarp and also producing a zone of liquefied mud below the scarp that flowed downhill. Within about 10 m of the main scarp the mud had lost sufficient water to become solid and resist the flow of liquefied mud above, though often buckling up to form a low ridge. The lower halves of the slump floors were dry, hard, and apparently quite stable, though still sparsely vegetated. Several of the slumps had alluvial fans below them consisting of sediment eroded from the slump. Sediment from the slumps caused a noticeable increase in turbidity in a few of the adjacent lakes.

A laterally extensive, debris-rich ice layer, interpreted as relict Pleistocene glacial ice, was exposed near the base of the main scarp in many of the study RTS. In moraines of the Itkillik II glaciation (the last glacial maximum, 14 to 25 thousand years ago) the ice was typically overlain by about 1.5 m of cobbly glacial till, and main scarps were about 2 m high. Some of the RTS in older deposits had large, Pleistocene ice wedges in addition to glacial ice. RTS with ice wedges had higher main scarps (8 to 10 m) and larger volumes of displaced material.

Examination of c. 1980 aerial photography showed that similar slumps had occurred prior to that time. The slumps that were active in 1980 are visible on 2008 satellite imagery (and at our 2010 visit), but most had revegetated after expanding little beyond their 1980 extent. Some of the currently active slumps studied in this report were advancing across land that had slumped in the past and then stabilized. Other slumps were advancing across land with no obvious signs of prior slumping. Only two of the study slumps appeared likely to have formed by continued migration of an escarpment that was active in 1980. The main scarps of the study slumps have migrated between 100 and 300 m in 30 years or less, indicating minimum migration rates of 3 m to 10 m per year. The goal of future monitoring of these slumps will be to determine their rates of growth or stabilization and revegetation, and to understand the factors that influence their growth, including the effects of ground ice types, geological setting, and weather.

Introduction

Retrogressive thaw slumps (RTS) are dramatic features of the arctic landscape caused by thaw of permafrost. They occur where a cut-bank in ice-rich permafrost advances into undisturbed ground as material thaws in the steep bank, falls or slides onto the adjacent more gentle slope, and then is transported away by viscous flow or water erosion (Burn and Lewkowicz, 1990). The advancing cut-bank, referred to here as the "main scarp" in keeping with standard landslide terminology (Beltran et al., 1993), is typically 2 to 10 m high. RTS often begin as escarpments produced by coastal, lakeshore, or fluvial erosion and then advance away from the shore by thaw and slumping, sometimes shedding large amounts of sediment into the adjacent water body. Very ice-rich material of substantial thickness (e.g. several meters) and lateral extent is needed to produce a RTS (Lacelle et al., 2010). Retrogressive thaw slumps are one of many phenomena produced by the action of thermokarst, which is subsidence caused by the thaw of ground ice (Czudek and Demek, 1970; Jorgenson and Osterkamp, 2005). RTS are among the most active of thermokarst landforms and result in the exposure of extensive areas of bare soil.

Mapping by Balser et al (2007), and an in-progress systematic inventory of RTS in ARCN by NPS (Swanson, 2010 and unpublished data for Noatak National Preserve, NOAT, and Gates of the Arctic National Park and Preserve, GAAR) has identified over 200 RTS in NOAT and GAAR. RTS are particularly common in the eastern part of NOAT (Fig. 1), and thus this area was emphasized in the initial year of our study.

While localized thaw and refreezing of permafrost occurs under a stable cold arctic climate, climate change has been cited as a cause of increased thaw of permafrost since 1982 in Alaska (Jorgenson et al., 2006). Concerns about the future state of permafrost led the National Park Service Arctic Inventory and Monitoring Network (ARCN, the five NPS units in northern and western Alaska) to include permafrost as a monitoring "vital sign" (Lawler et al., 2009). Thaw-related slumping and associated soil erosion may have increased in ARCN in recent years (Balser et al., 2007), and an important component of ARCN's permafrost vital sign monitoring involves intensive monitoring of selected thaw slumps. The activity of RTS in some areas of Canada has increased in recent decades (Lantuit and Pollard, 2008; Lantz and Kokelj, 2008).

Because RTS are large erosion features that often occur near water bodies, they can affect water quality. Suspended sediment, ions in solution, and pH have been shown to be higher below RTS and other thermokarst erosion features (Bowden et al., 2008; Crosby, 2009; Kokelj et al., 2005). Ions that increase include nutrient species such as potassium, phosphate, sulfate, ammonium, and nitrate, as well as other common soil cations such as calcium, magnesium, and sodium.

The present study utilizes aerial photography to create 3-dimensional models of selected slumps in ARCN. On future visits we will re-photograph these slumps and create new 3-D models that can be compared to the baseline models shown here, allowing us to calculate area, rates of slump expansion, volume of material displaced, and rates of revegetation.

Methods

Site Selection

RTS were selected from mapping of permafrost-related erosion features in ARCN (Swanson, 2010; and Swanson, in preparation) and previous work by Balser et al (2007)(Table 1). All are within the zone of continuous permafrost (Jorgenson et al., 2008). Permafrost temperatures here are unknown, but the mean annual air temperature at the Noatak RAWS (located about 25 km east of slumps NOAT004, -039, and -040 and at a lowland elevation similar to all the slumps) for the period 1990-2010 was -6.5°C (Jan mean -25.7°, July 13.2°; WRCC, 2010). RTS were selected for intensive photographic monitoring based on 1) size, 2) potential for siltation of adjacent water bodies, 3) potential for encroachment on archeological sites, 4) visual impact, and 5) proximity to other slumps (for economy of access). The concentration of sites studied in the eastern part of NOAT reflects the abundance of slumps in this region and proximity to our base of helicopter operations in 2010 near Kobuk, Alaska, (located just south of the area depicted in Fig. 1). Twenty-four slumps were photographed in 2010 and will be supplemented with other sites in future years for an expected total set of 25 to 30 RTS that will be followed with long-term monitoring. In the future we intend to add additional monitoring sites at slumps outside of the current study area, in the western half of NOAT and further east in GAAR. The study slumps will be re-photographed at intervals of 1 to 5 years, depending on the rate of change, funding, and logistical considerations.

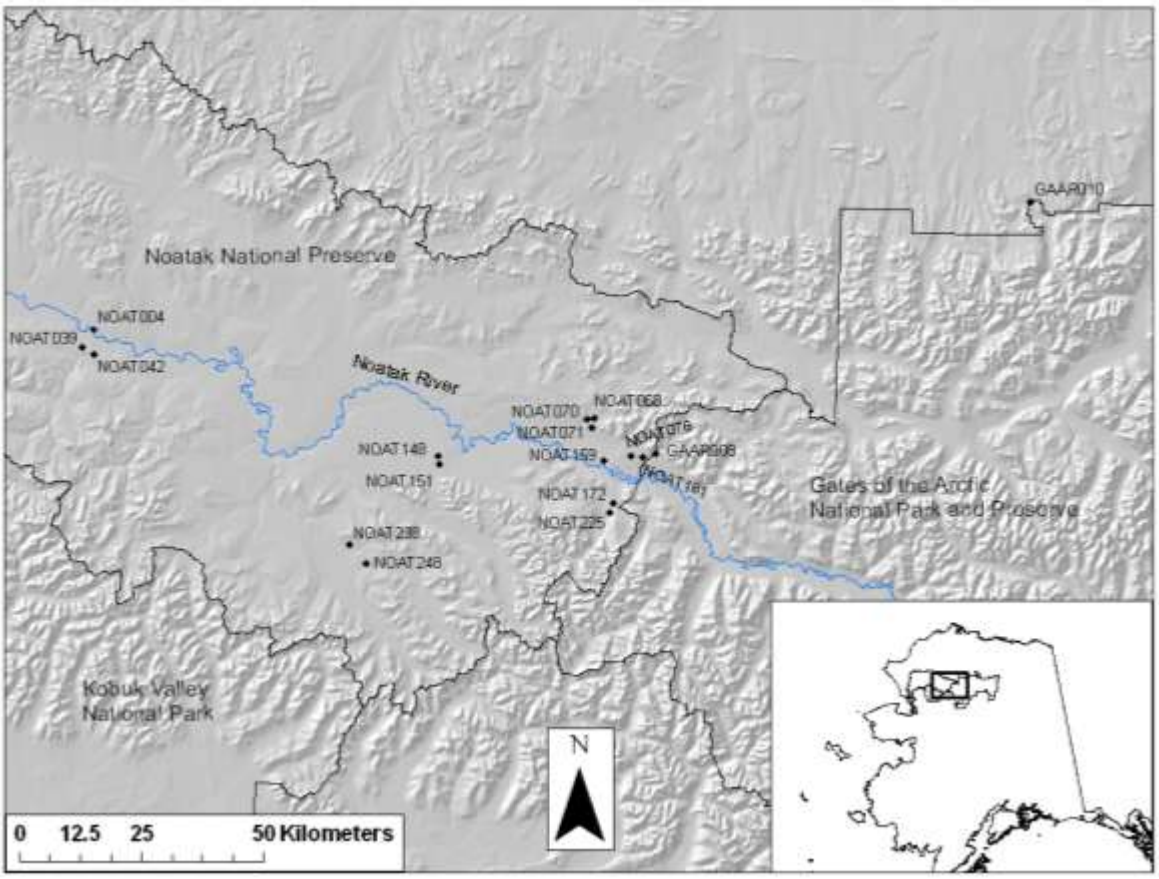

Figure 1. Location map of retrogressive thaw slumps photographed in 2010.

Table 1. Retrogressive thaw slumps photographed in 2010.

Slump identifier	Longitude, deg-min W (NAD83)	Latitude, deg-min N (NAD83)	Ground Control 2010
GAAR008	156° 29.17’	67° 54.04’	√
GAAR010	154° 40.81’	68° 22.99’	√
NOAT004	159° 14.65’	68° 04.22’	
NOAT039	159° 17.48’	68° 02.15’	√
NOAT042	159° 14.08’	68° 01.43.’	√
NOAT068	156° 47.30’	67° 57.66’	√
NOAT069	156° 47.56’	67° 57.64’	√
NOAT070	156° 49.42’	67° 57.50’	√
NOAT071	156° 48.02’	67° 56.56’	√
NOAT072	156° 48.40’	67° 56.62’	
NOAT073	156° 49.14’	67° 56.85’	
NOAT074	156° 36.03’	67° 53.87.’	
NOAT076	156° 36.27’	67° 53.66’	
NOAT148	157° 31.94’	67° 52.61’	√
NOAT151	157° 31.60’	67° 51.77’	√
NOAT159	156° 44.15’	67° 52.98’	
NOAT160	156° 44.12’	67° 52.87’	
NOAT161	156° 32.86’	67° 53.61’	√
NOAT172	156° 40.90’	67° 48.39’	√
NOAT225	156° 41.59’	67° 47.25’	√
NOAT237	157° 56.12’	67° 42.30’	
NOAT238	157° 56.16’	67° 42.24’	
NOAT247	157° 51.10’	67° 40.18’	√
NOAT248	157° 51.17’	67° 40.24’	√

Ground Survey and Photography

Sites were accessed by helicopter or floatplane. We landed at 12 locations (which provided access to 16 slumps) and surveyed ground control points around the perimeter of the feature using a Topcon 235W total station. This instrument provides sub-centimeter accuracy in location (including elevation) relative to the survey instrument. Typically 5 ground control points were surveyed, and each point was marked with an aerial marker, as was the station location, for a total of 6 control points. The absolute location of the total station was determined using differentially corrected GPS, for an accuracy of about 1 m. All elevations are reported here in meters relative to the total station location, which was at the upper end of the slump at all locations except GAAR008.

With the aerial markers in place, oblique aerial photographs were shot out the window or door of the aircraft using a Nikon D700 camera, which has a “full-frame” (35 mm) sensor, with a 50 mm lens. Photos were shot on multiple linear passes over the RTS; passes were oriented to completely cover the RTS and surrounding undisturbed ground, and to provide detail of vertical faces with various orientations. Consecutive photos overlap to provide stereo coverage of the entire slump and adjacent areas; stereo coverage is needed to produce 3-dimensional models.

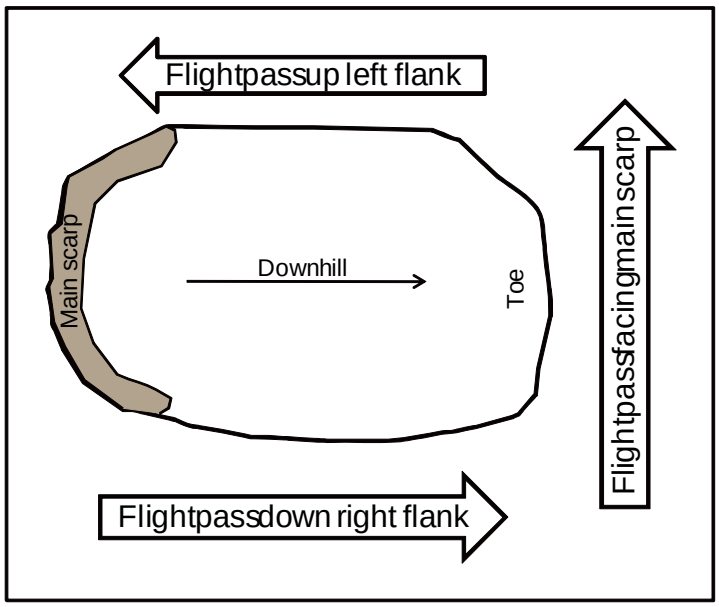

Typical flight pass orientations with photos taken out of the left side of the aircraft are shown in Fig. 2. Passes facing the main scarp were made at close range, across the middle of the slump, to view detail of the main scarp and upper slump; or from below the toe to view the whole slump. An example of two photos taken during a flight pass down the right flank of a slump (NOAT142) is given in Fig. 3.

Figure 2. Configuration of typical flight paths for slump photography.

Figure 3. Consecutive photographs of slump NOAT142, shot out of the left side of a helicopter during a flight pass down the right flank. A ground control point, marked with white “X” on a black square that is 1.5 m on a side, is visible near the lower left edge of the slump in the left photograph.

3D Model Construction and Data Analysis

Three-dimensional models of the RTS were constructed from oblique aerial photographs using Topcon Image Master software (www.topconpositioning.com). Common points identifiable on pairs of adjacent photos (known as "pass points") and the aerial markers with known coordinates (ground control points) were located on the photos. Image Master used these points to determine the location and orientation of the camera when each photo was taken. The computation of camera locations was by bundle adjustment, which means that all photos, pass points, and ground control points were used simultaneously to compute the solution. Then a 3-dimensional surface was constructed in Image Master as follows: a grid spacing was chosen (typically 2 m), and the software located grid points on one photo, then by image correlation located the same features on the next photo in the flight line. From the camera orientation and shift in location between the two photographs, the software calculated the 3D location (x, y, and z) of each grid point. The points were then used to create a triangular interpolated network (TIN), which is a 3D surface comprised of the triangles created by lines joining the points (Fig. 4). The photos were projected onto the TIN to create a realistic 3D model (Fig. 4). This model was used to create orthophotographs (photographs with map view and all perspective and elevation distortions removed) and cross-sectional diagrams, and to calculate slump area, main scarp height, slope, and volume. The orthophotographs and cross-sectional diagrams are all displayed so that the slump slopes downhill from left to right.

The camera location and accuracy parameters reported in this report are described below and reported in a table in the results section for each slump (Tables 3 through 15). The average, minimum and maximum for each parameter were computed for the set of all photos in the pass indicated in the table.

Camera elevation, m – the elevation of the camera relative to the total station location (which is also the zero level on the cross-sectional diagram).

Camera angle ω, in degrees from vertical

Distance to target, m – This is the distance to the ground at the center of the photograph

Base:height ratio – the ratio between the distance traveled between photos and the distance to target. Wider ratios (greater than 0.2) provide better elevational accuracy, but result in slivers between photos without overlap, and thus without topography, in the foreground

Control point error in x, m – the *average* is the root mean square error of the computed location of the ground control points (by the bundle adjustment) in the x direction (east-west) relative to their actual location as determined by ground survey. The *maximum* is the greatest difference between a control point's measured location and its location computed by the bundle adjustment.

Control point error in y, m – as above, except the error is in the y direction (north-south)

Control point error in z, m – as above, except the error is in the elevation.

Distances to the target were typically 200 to 300 m, which yielded pixel sizes averaging 3 to 5 cm at the photo center but varying greatly between the foreground and background. The camera angle from vertical was generally 50° to 65°; steeper angles are preferred but the view steeper than 50° was obscured by landing gear. The base:height ratio ranged from 0.1 to 0.3. Control point errors averaged less than 0.1 m for x, y, and z in most models

In the future, photographs will be re-taken in a similar fashion at all sites. At sites where ground control was obtained in 2010, landing will not be needed in the future, greatly reducing the expense. The new photos will be registered to the photos from the previous visit using landmarks visible on both photo dates, and ground control information will be transferred to the newer photos. In other words, the 2010 photos will be used to determine the location, scale, and level in the newer photos, and then new 3D models will be constructed with the new photos. These new models will be compared to the previous visit(s) to determine the rate of growth or revegetation of the RTS.

At four sites, photographs were taken but time constraints prevented us from landing and gathering ground control data in 2010. However, we plan to place ground control at these localities in the future, and landmarks will be used to transfer the ground control information back to the 2010 visit. Thus sites without ground control in 2010 will provide the same 3-D models and capability for change detection as those surveyed in 2010.

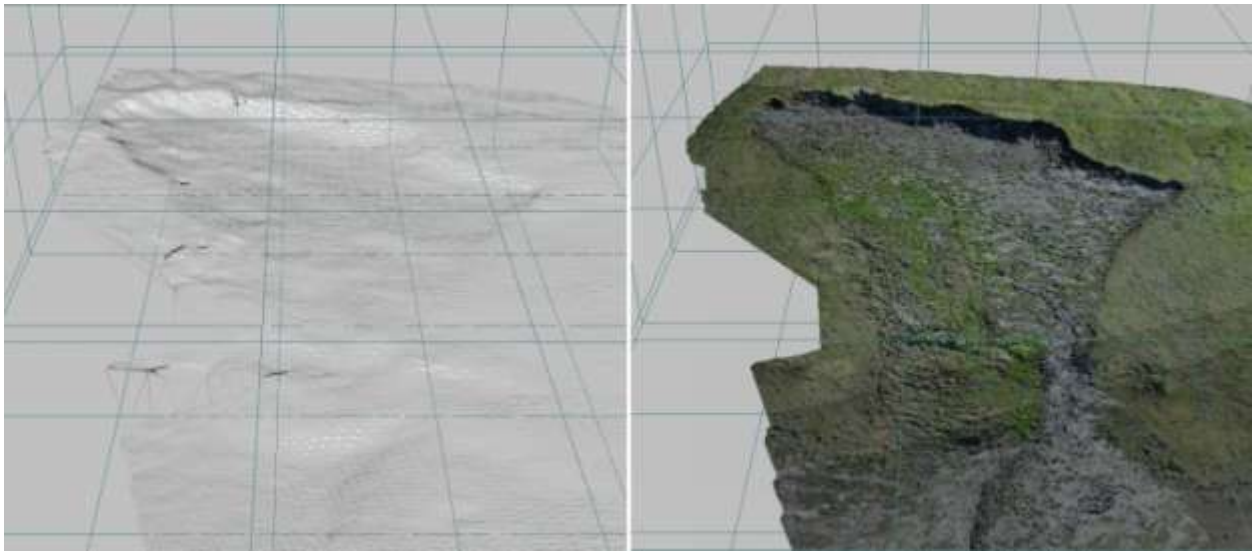

Figure 4. Construction of a three-dimensional model (slump NOAT142). On the left is a triangular interpolated network (TIN) constructed by connecting points with x-y-z coordinates determined by shift between adjacent images. On the right is the TIN with photographic overlay. A stereo photo pair from the line of photos used to create this model is shown in Fig. 3.

Results

The study RTS occur on moderate slopes of about 10%. They ranged in area from less than 1 ha to over 4 ha and have main scarps 1 to 10 m high (Table 2). A range of aspects is present, though only one slump faced south (Table 2). The main scarps were typically nearly vertical at the top, with a steep slope of sediment and pieces of intact sod below the vertical face. In most slumps there was a zone of liquefied mud extending downslope away from the base of the main scarp. The mud became firmer with distance from the main scarp, such that the liquefied zone was typically less than 10 m wide in late June. In some cases the firmer material was deformed into a low ridge parallel to the main scarp, with fractures indicating upward buckling due to compression by the flowing mud above. The slump floors beyond the liquefied zone and adjacent compression zone were dry, firm, and showed no fresh deformational fractures, though rivulets and small gullies indicating surface water erosion were common.

The height of the main scarp was related to the type of ground ice present, which was in turn related to the age of the material in which the slump formed. The retrogressive thaw slumps with the tallest main scarps (greater than 5 m tall, Table 2) had large ice wedges in addition to glacial ice. Exposures with both buried glacial ice and ice wedges were found in places that were glaciated during the Anisak or Itkillik I glaciations and then left exposed during the late glacial maximum (Itkillik II). The slumps in Anisak glacial till were the only ones with distinct wind-deposited (eolian) layers (loess) on the surface. On the youngest moraines (Itkillik II), we found lower main scarps exposing glacial till over glacial ice, and ice wedges were not present.

Table 2. Slump areas, main scarp heights, aspects, ice types, and geological settings.

Slump Name	Main scarp height, m[1]	Slump area, ha	Aspect[2]	Massive ground ice types[3]	Geological setting
NOAT039	10	4	ENE	Wedge and glacial	Eolian over Anisak glacial till
NOAT042	10	1.7	N	Wedge and glacial	Eolian over Anisak glacial till
NOAT172	10	2.1	NW	Wedge and glacial	Itkillik I glacial till
NOAT148	8	1.7	WNW	Wedge and glacial	Itkillik I glacial till
NOAT068	5	2.4	N	Glacial	Itkillik I glacial till
NOAT071	5	0.7	N	Not exposed	Itkillik I glacial till
NOAT225	5	1.2	W	Not exposed	Itkillik I glacial till
NOAT247	5	0.8	ENE	Not exposed	Itkillik I glacial till[4]
NOAT151	4-5	4.4	ENE	Glacial	Itkillik I glacial till
NOAT070	4	3.5	W	Glacial	Itkillik I glacial till
NOAT161	2	1.4	WNW	Glacial	Itkillik II glacial till
GAAR008	2	1.1	WNW	Glacial	Itkillik II glacial till
GAAR010	1-2	2.5	S	Not exposed	Itkillik II glacial till

[1]The maximum height different between the undisturbed surface above the main scarp and the gently sloping floor.
[2]E – east, N – north, S – south, W – west.
[3]Wedge ice consisted of large, dark-colored ice bodies lacking any coarse fragments and interpreted as wedges that formed during Pleistocene (more than 10,000 years ago) cold periods. These wedges were several meters wide, separated by mineral soil, and extended several meters downward from the active layer. Smaller Holocene (10,000 years to the present) ice wedges were also observed at slump NOAT039. Glacial ice consisted of ice with suspended sand, pebbles, and cobbles, forming a continuous layer near the bottom of the section, often with horizontal stratification.
[4]Glacial advances are named as follows (Hamilton, 2009). Anisak – western Brooks range advance correlated with the Itkillik I of the central Brooks Range. Itkillik I – older than 40 thousand years, probably 60-100 thousand years. Itkillik II – last glacial maximum, 14-25 thousand ^{14}C years ago.
[4]Mapped by Hamilton as glaciolacustrine deposits but interpreted in the field as glacial till

GAAR008

GAAR008 is in an extensive disturbed area along Douglas Creek, which forms the border between NOAT and GAAR (Figs. 5-7). The active slump covered about 1.1 ha, with an additional 0.5 ha in associated fans. It is on Itkillik II glacial till (Hamilton, 2009). The bare areas adjacent to the active slump appear to be partially revegetated older slumps. Ground control in 2010 was placed across this disturbed area and the lower part of the active slump, but not around the active slump's periphery, which reduced the accuracy of the model of the active slump. (Thus we will not report slump volume here and have planned a return visit to obtain better ground control.) The active slump was on a slope of about 10% with west-northwest aspect. The main scarp was about 2 m high and exposed debris-rich glacial ice below glacial till (Fig. 7). The liquefied zone near the main scarp had a slope of less than 10%, but the slope of the floor of the active slump averaged about 10%. GAAR008 began at an inactive escarpment from an older slump sometime after 1977 (Fig. 5)

Table 3. Camera location and accuracy parameters for GAAR008[1].

Parameter	Mean	Minimum	Maximum
Pass 2010A			
Camera elevation, m	166	148	190
Camera angle ω, ° from vertical	56	50	59
Distance to target, m	412	340	474
Base:height ratio	.014	0.09	0.21
Control point error in x, m	0.066		0.092
Control point error in y, m	0.049		0.070
Control point error in z, m	0.074		0.102

[1]12 photos, 3 control points

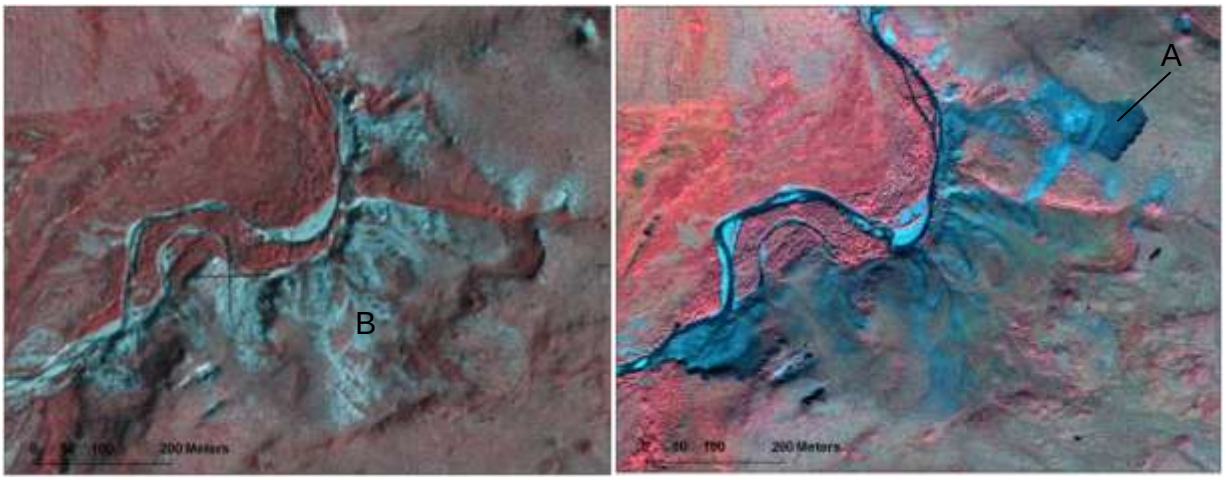

Figure 5. Slump GAAR008 in 1977 (left, AHAP aerial photograph) and 2008 (right, IKONOS imagery). Here and all further AHAP and IKONOS images have the traditional color-infrared color scheme, where green reflectance is rendered as blue, red reflectance as green, and near infrared reflectance as red. The currently active slump (A) grew from a slump escarpment that had stabilized prior to 1977. The extensive sparsely vegetated areas (B) are inactive slumps that changed very little in 31 years.

Figure 6a. Orthophotograph of slump GAAR008, constructed from pass 2010A. For scale see the cross-section (Fig. 6b), which follows the line in Fig. 6a.

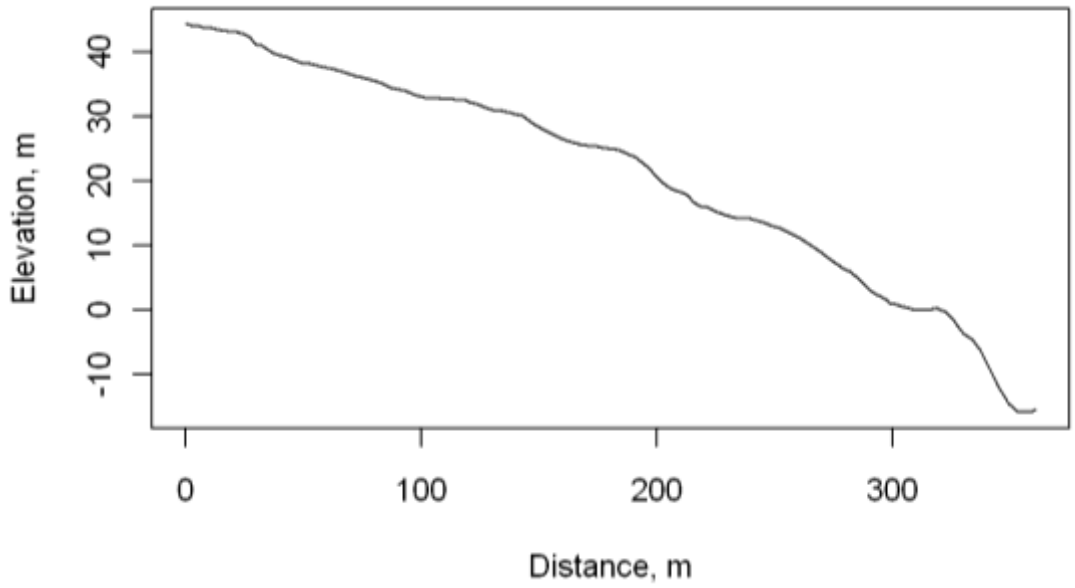

Figure 6b. Cross-section of slump GAAR008, The cross-section alignment is indicated on Figure 6a. Beyond about the 170 m distance the section crosses partially vegetated areas that are probably older slumps.

Figure 7. Main scarp of slump GAAR008. The scarp exposes about 1.5 m of glacial till (A), over debris-rich glacial ice (B). A zone of liquefied mud is present just below the scarp (C), with floating rafts of intact vegetation (D).

GAAR010

GAAR010 is a large, (2.5 ha), shallow slump on a south-facing slope of about 10% located near Kurupa Lake in northern GAAR (Figs. 8-10). The geologic material is Itkillik II glacial till (Hamilton, 1980). The main scarp was indistinct and only 1 to 2 m high (Fig. 10). Large strips of vegetation were detaching and sliding intact. The slope of the slump floor averaged about 10%, gradually increasing from top to bottom. A small gulley extended down the toe of the slump to the Kurupa River, but it was dry on 15 July 2010. The volume of the depression in the upper part of the slump where it is fairly distinct was about 2,200 m^3 over an area of about 0.35 ha for an average depth of less than 1 m. In 1982 there was no active slumping or obvious revegetated slumps in the vicinity of GAAR010, based on AHAP aerial photography, indicating that this nearly 300 m-long slump formed in less than 30 years.

Table 4. Camera location and accuracy parameters for GAAR010[1].

Parameter	Mean	Minimum	Maximum
Pass 2010B			
Camera elevation, m	117	114	119
Camera angle ω, ° from vertical	50	47	51
Distance to target, m	247	231	266
Base:height ratio	0.11	0.10	0.15
Control point error in x, m	0.022		-.045
Control point error in y, m	0.024		.038
Control point error in z, m	0.024		-.032

[1]16 photos, 6 control points

Figure 8. Overview of GAAR010 on 2007 IKONOS imagery.

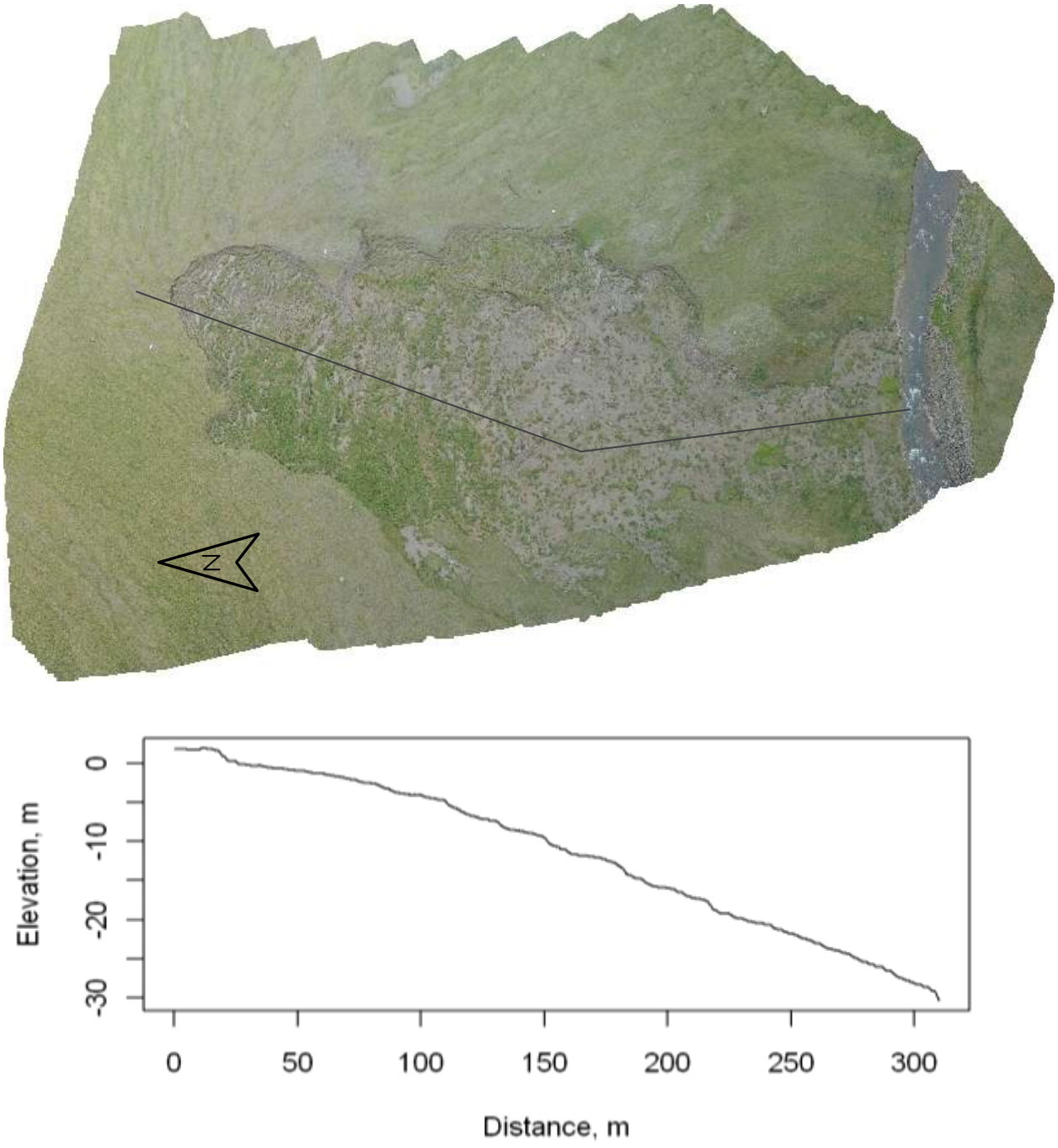

Figure 9. Orthophotograph and topographic cross-section of slump GAAR010, constructed from pass 2010B. Here and in all subsequent orthophotos and cross-sections, the orthophotograph is oriented so that the slump slopes downhill to the right, the position of the cross-section is given by a line on the photo, and the scale of the photo is provided by the horizontal scale on the cross-section. The vertical scale on the cross-section is exaggerated with respect to the horizontal scale.

Figure 10. Main scarp region of slump GAAR010.

NOAT004

NOAT004 is a small, west-facing slump with overhanging main scarp on a bluff above the Noatak River (Fig. 11). It is located above an unvegetated slope that was not actively subsiding, but was steepened by erosion of the Noatak River. Revegetated slumps in positions similar to NOAT004 were visible on either side. NOAT004 was photographed without ground control in 2010. AHAP photography from 1978 reveals bare river bluffs with an active slump close to today's NOAT004, and multiple revegetated slumps.

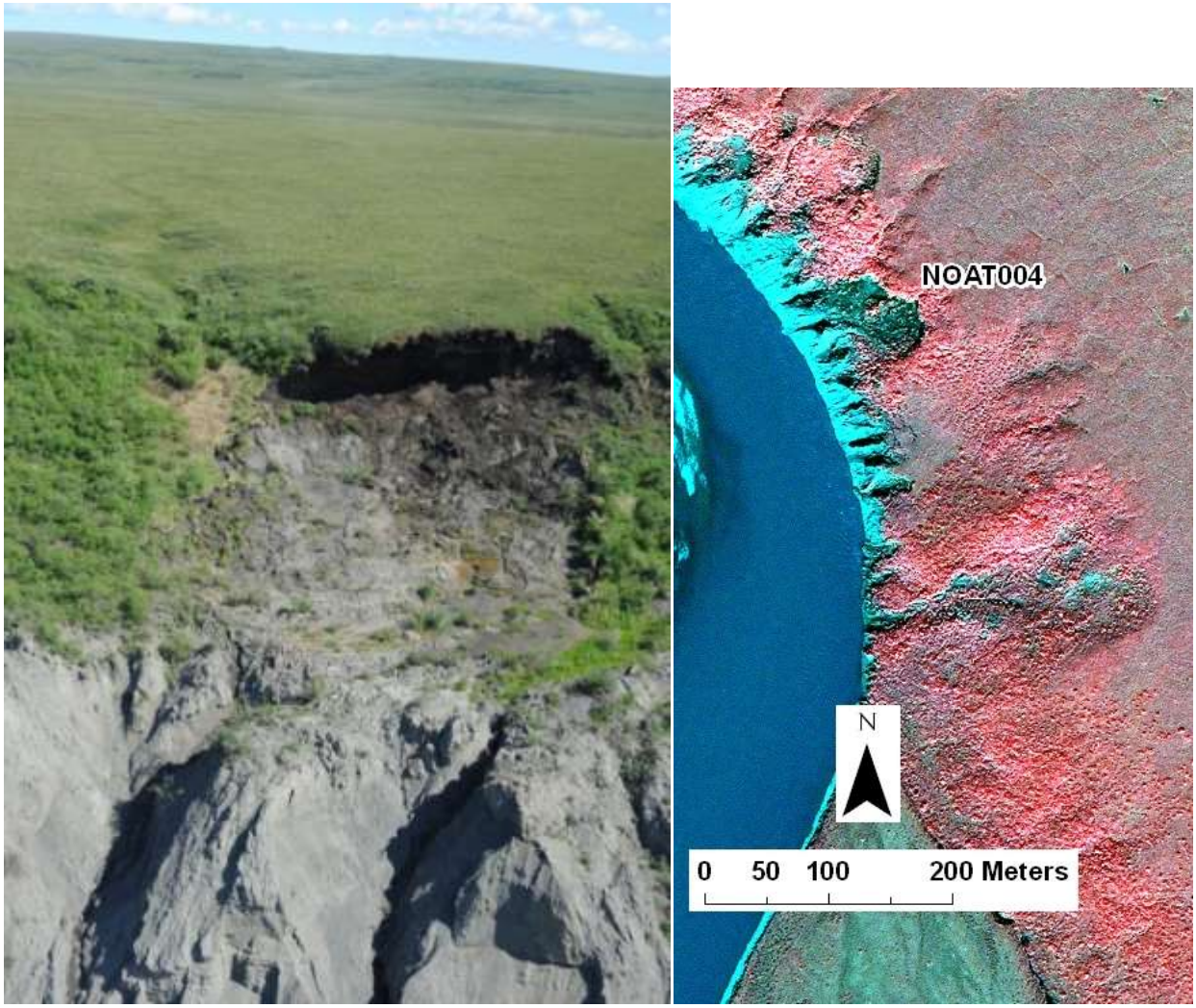

Figure 11. Slump NOAT004, small-format oblique aerial photograph (left) and August 2007 IKONOS satellite image, color-infrared color scheme.

NOAT039

NOAT039 is a large, east-northeast facing slump on a slope of about 9% along a small lake near Lake Kangilipak in the middle Noatak Valley (Figs. 12-15). It is on Anisak glacial deposits (Hamilton, 2009) covered by several meters of finer wind-deposited sediment (loess). It had an area of about 4 ha and main scarp about 10 m high with spectacular ground ice exposures. In the upper area of 3.5 ha that formed a distinct depression, the estimated volume loss was about 160,000 m^3. The main scarp ice exposures revealed large Pleistocene ice wedges (formed during the last glacial cold period, more than 10,000 years ago) formed in the loess and underlying glacial till (Fig. 14). These wedges were identified as Pleistocene age by their size, and dark color caused by included eolian sediment. These wedges cut into glacial ice found under the till, and they were in turn cut by smaller Holocene (less than 10,000 yr-old) ice wedges. Holocene ice wedges in upland sites such as this are considerably smaller than Pleistocene wedges and the ice is relatively pure and thus white-colored. The main scarp was high, steep, and actively eroding, with a zone of supersaturated mud 10-15 m wide near its foot. Slopes near the main scarp were 10-20%; below this the sediment was drier and firmer, and buckled up in response to pressure from above, forming a step-like feature (between the 35 and 40 m marks on the cross-section Fig. 12). The main floor of the slump had an average slope of about 5%, becoming steeper near the lakeshore. NOAT039 has re-occupied the site of prior slumps that had revegetated before 1980. In 1980 there was a small slump in what is now the toe of NOAT039 that is probably an early phase in its formation.

Pass A faces the main scarp from fairly close range and covers the upper half of the slump; it provides detail of the main scarp region. Pass B also faces the main scarp but is centered lower down on the slump and covers all except the lowest part of the slump.

Table 5. Camera location and accuracy parameters for NOAT039[1].

Parameter	Mean	Minimum	Maximum
Pass 2010A			
Camera elevation, m	117	99	139
Camera angle ω, ° from vertical	50	47	53
Distance to target, m	240	192	310
Base:height ratio	0.14	0.11	0.18
Control point error in x, m	0.017		.027
Control point error in y, m	0.009		-.014
Control point error in z, m	0.019		.027
Pass 2010B			
Camera elevation, m	98	91	107
Camera angle ω, ° from vertical	54	52	55
Distance to target, m	258	207	311
Base:height ratio	0.13	0.09	0.19
Control point error in x, m	0.052		-0.111
Control point error in y, m	0.092		-0.138
Control point error in z, m	0.039		.066

[1]Pass 2010A - 12 photos, 6 control points; pass 2010B - 12 photos, 6 control points

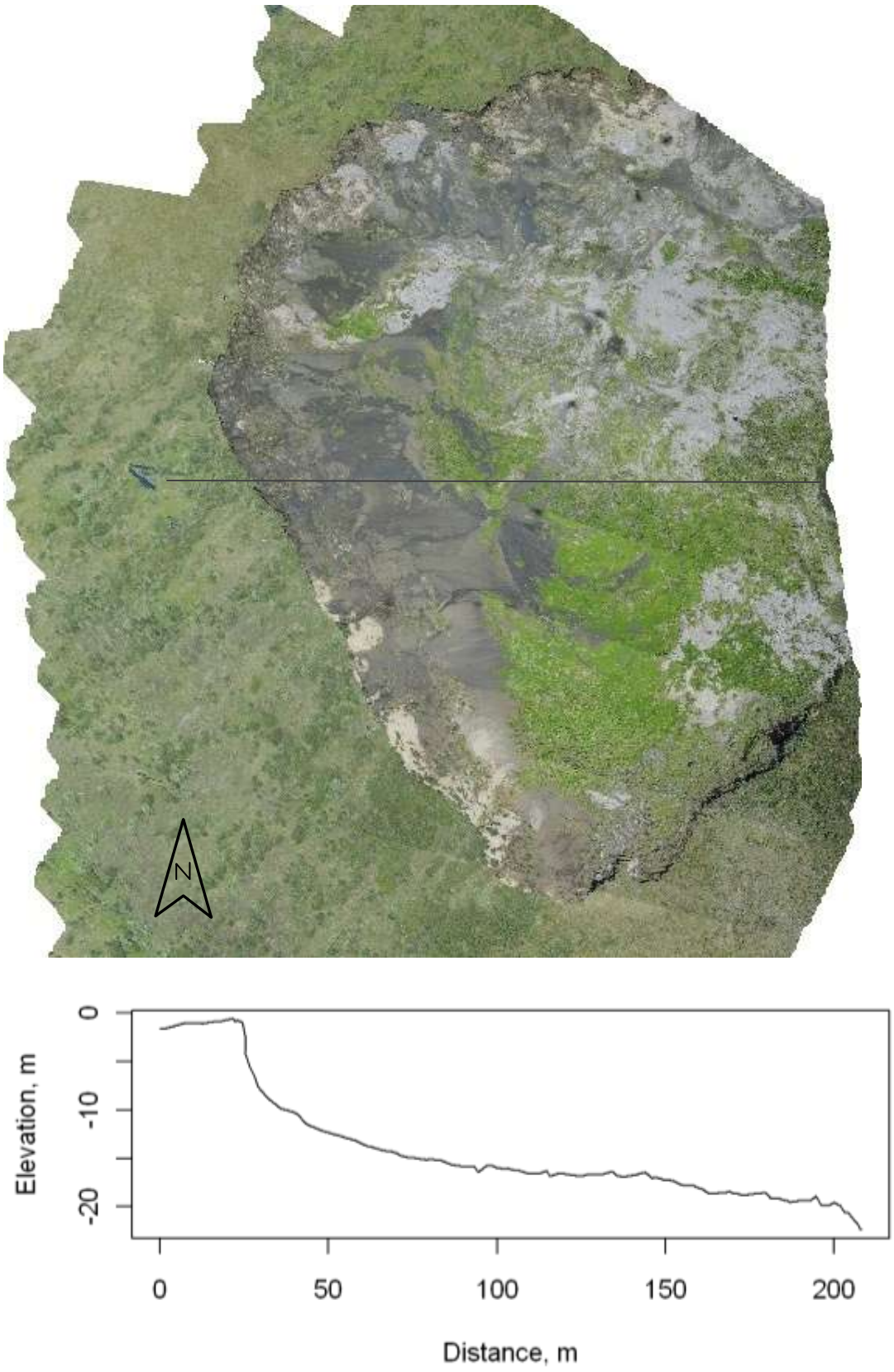

Figure 12. Orthophoto and topographic cross-section of slump NOAT039, constructed from pass 2010B.

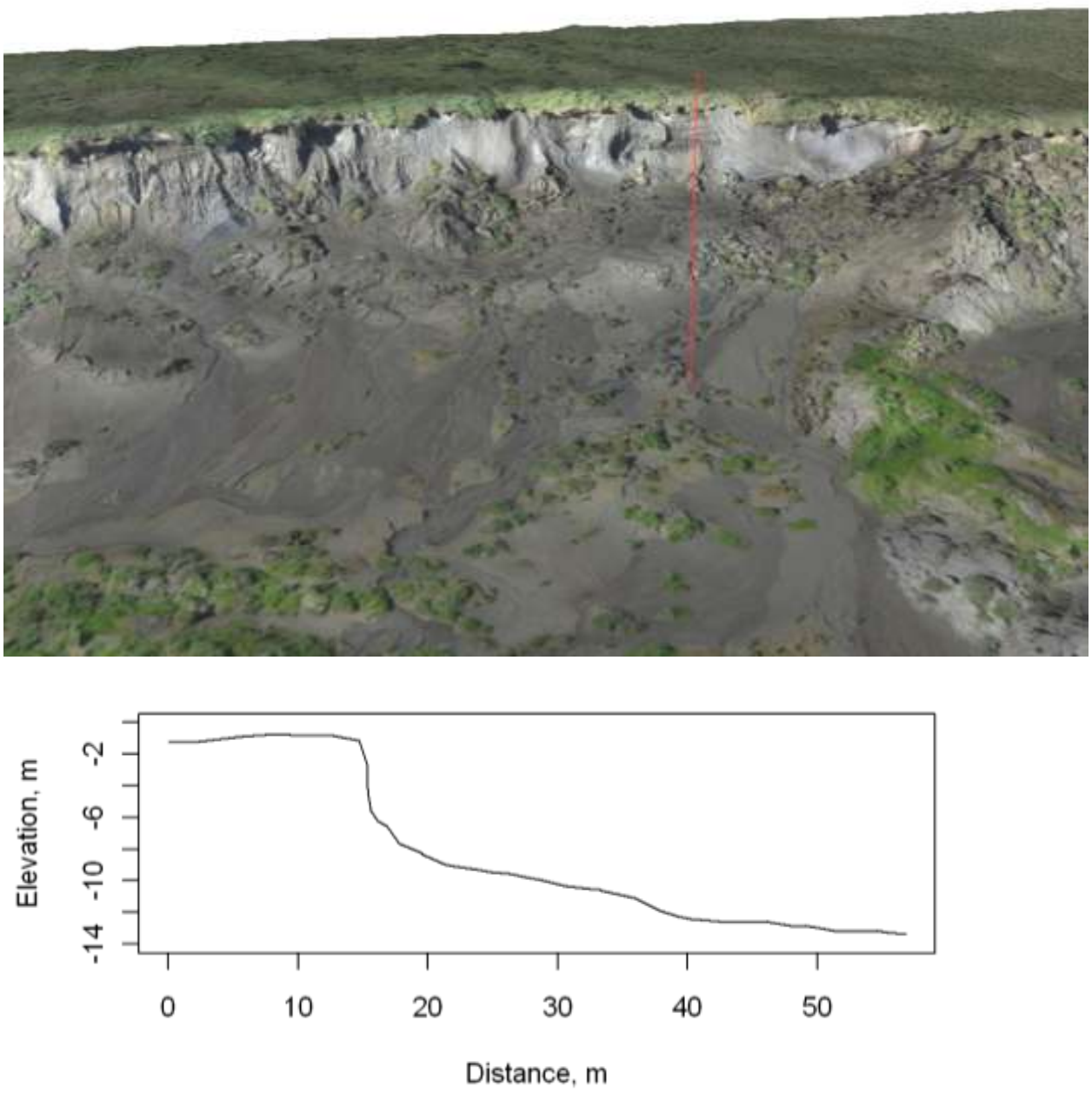

Figure 13. Synthetic close-up of main scarp region of NOAT039 with topographic cross-section, constructed from pass 2010A. The image was constructed by draping multiple photographs over the TIN and tilting the view to simulate an oblique aerial photograph.

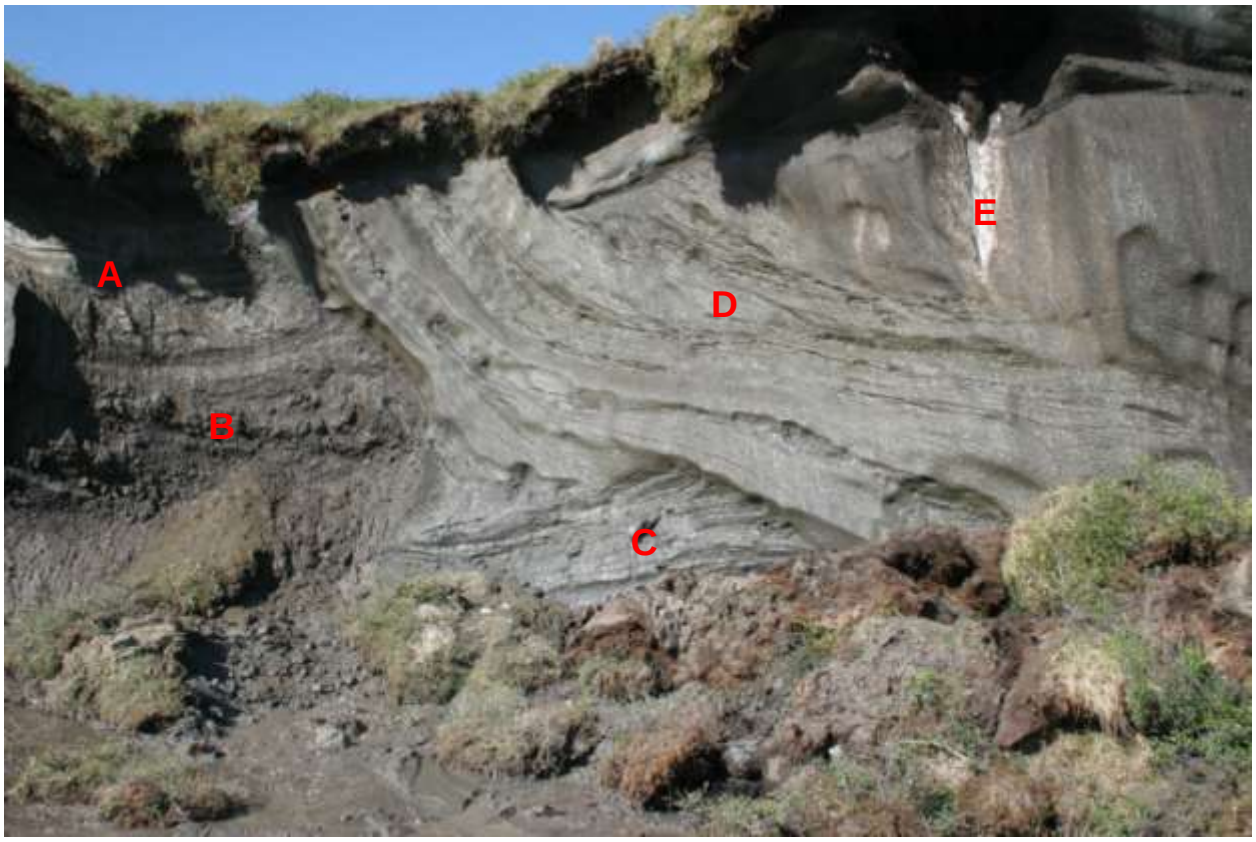

Figure 14. Ground ice exposed in the main scarp of slump NOAT039. The red cross-section line in Fig. 13 passes across the left side of the photograph. A – frozen wind-deposited sediment. B – frozen glacial till. C – Pleistocene glacial ice. D – Pleistocene ice wedge. E – Holocene ice wedge.

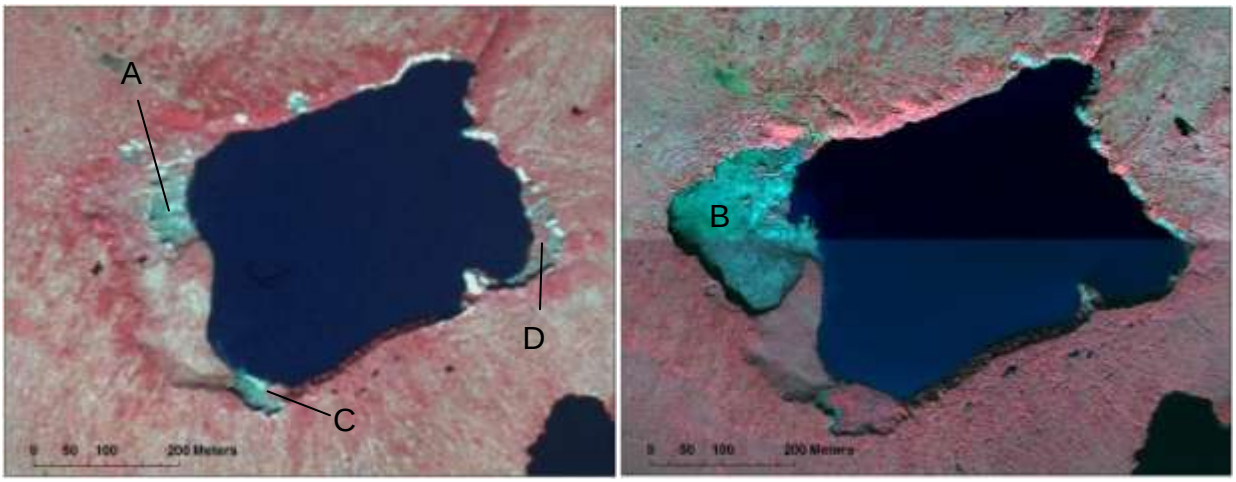

Figure 15. Slump NOAT039 in 1980 (left, AHAP aerial photography) and 2007 (right, IKONOS imagery). A vegetated gentle scarp outlining a depression along the whole western side of this lake in 1980 indicates past slumping. Gray tones near the shore in the northwest corner of the lake in 1980 (A) suggest initiation of the present-day larger slump NOAT039 (B). Other developments in this very active area include expansion of the slump at C followed by nearly complete revegetation, and subsidence at D resulting in expansion of the lake.

NOAT042

NOAT042 is a north-facing slump on a slope of about 14%, along a lake margin at the western edge of the study area, in Anisak glacial till deposits (Figs. 16-18). Comparisons between 2007 IKONOS imagery and 1980 AHAP photography indicate that the perimeter of this lake has slumped and revegetated repeatedly in the past (Fig. 16.). Inactive areas have revegetated with shrubs. The main scarp had a maximum height of 10 m and exposed Pleistocene wedge ice, loess, and debris-rich glacial ice (Fig. 18). Below the vertical upper main scarp composed of ice wedges and glacial till, the slope decreased to 40-50° through intermittent areas of exposed glacial ice and liquefied mud. Between this zone and the lake perimeter, the ground hardened and the slope flattened to around 10%. The slump volume was about 52,000 m^3 over an area of 1.7 ha.

Table 6. Camera location and accuracy parameters for NOAT042[1].

Parameter	Mean	Minimum	Maximum
Pass 2010A			
Camera elevation, m	50	49	53
Camera angle ω, ° from vertical	68	66	70
Distance to target, m	236	219	250
Base:height ratio	0.11	0.09	0.12
Control point error in x, m	0.0014		0.0041
Control point error in y, m	0.0009		0.0029
Control point error in z, m	0.0008		0.0016

[1]7 photos, 6 control points

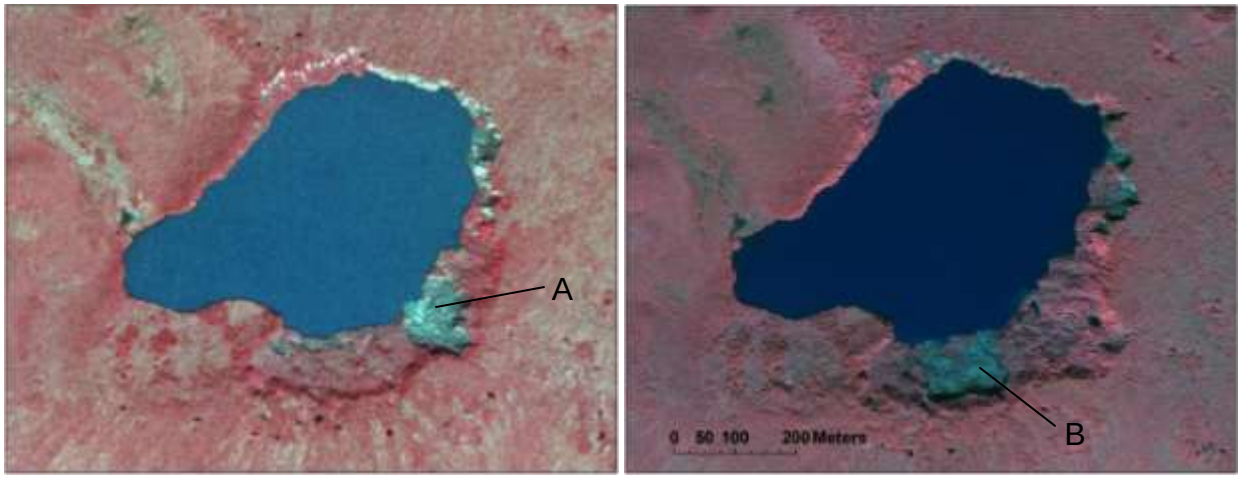

Figure 16. Slump NOAT042 in 1980 (left, AHAP aerial photography) and in 2007 (right, IKONOS imagery). Revegetated slumps surround much of this lake. The main active area in 1980 on the southeast shore (A) grew beyond the gray area visible in 1980 before revegetating. The currently active area of slump NOAT042 on the south shore (B) is re-occupying an area that had slumped and revegetated before 1980.

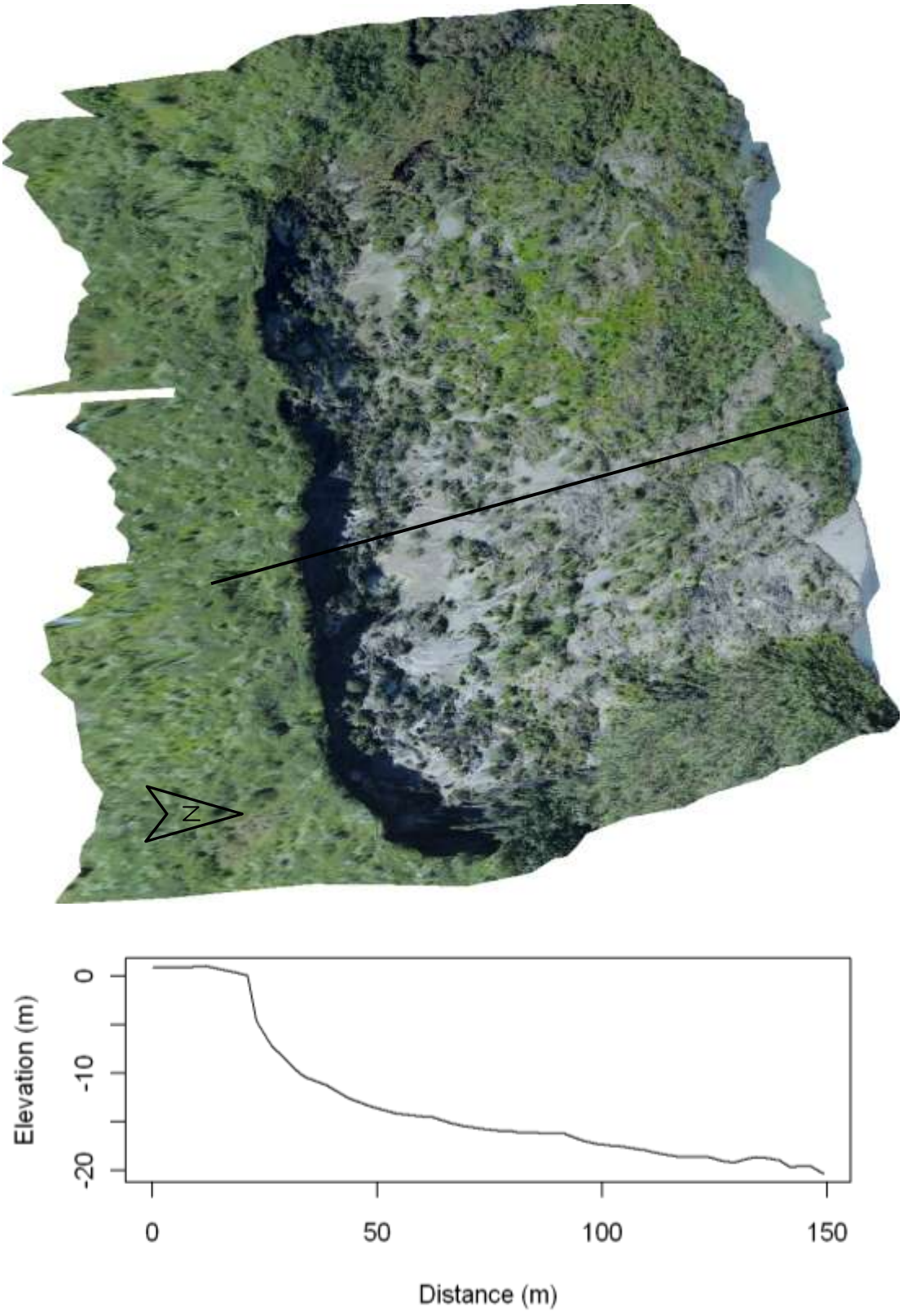

Figure 17. Orthophoto and topographic cross-section of slump NOAT042, constructed from pass 2010B.

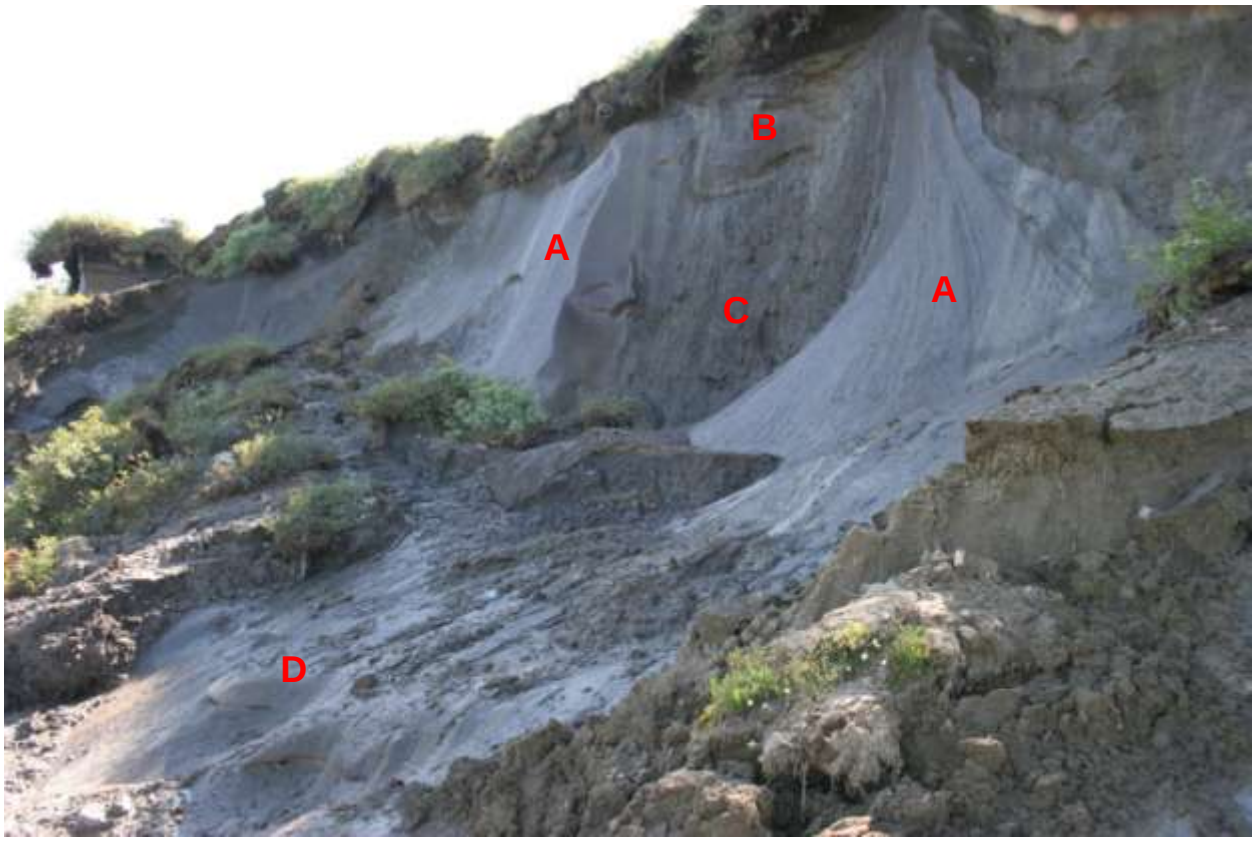

Figure 18. Photograph of the main scarp of slump NOAT042, exposing Pleistocene ice wedges (A) in loess (B) over glacial till (C). In a few places underlying debris-rich glacial ice (D) is exposed at the base of the section.

NOAT068 and NOAT069

NOAT068 and NOAT069 are two neighboring slumps on a slope of about 12% with north–facing aspect (Figs. 19-22). They are on Itkillik I glacial till (Hamilton, 2009). The larger of the two slumps (NOAT068) had an area of about 2.4 ha and a main scarp that was about 5 m high at its highest point. This main scarp exposed about 1.5 m of glacial till over debris-rich glacial ice (Fig. 21). The slope in the liquefied zone just below the thawing glacial ice was 5-10%. Below this the slope formed a series of steps separated by treads with slopes of 5% or less, producing an overall slope of about 17% on the slump floor. The distinct depression in the upper part of the slump had a volume of about 11,825 m^3 over an area of about 0.87 ha. The smaller slump (NOAT069) had an area of about 8230 m^2, a lower main scarp (2-3 m high) and gentler slope of about 10%. There are inactive slumps in the vicinity of NOAT068 and NOAT069, but AHAP aerial photography from 1977 shows the current extent of both slumps was undisturbed at that time.

Table 7. Camera location and accuracy parameters for NOAT068 and NOAT069[1].

Parameter	Mean	Minimum	Maximum
Pass 2010B			
Camera elevation, m	195	184	201
Camera angle ω, ° from vertical	50	46	56
Distance to target, m	377	365	384
Base:height ratio	0.22	0.19	0.23
Control point error in x, m	0.020		-0.035
Control point error in y, m	0.024		-0.031
Control point error in z, m	0.023		0.035
Pass 2010C			
Camera elevation, m	92	82	98
Camera angle ω, ° from vertical	49	47	52
Distance to target, m	245	223	260
Base:height ratio	0.21	0.19	0.25
Control point error in x, m	0.071		-0.131
Control point error in y, m	0.077		0.134
Control point error in z, m	0.060		-0.096

[1]Pass 2010B - 6 photos, 6 control points; pass 2010C – 9 photos, 6 control points

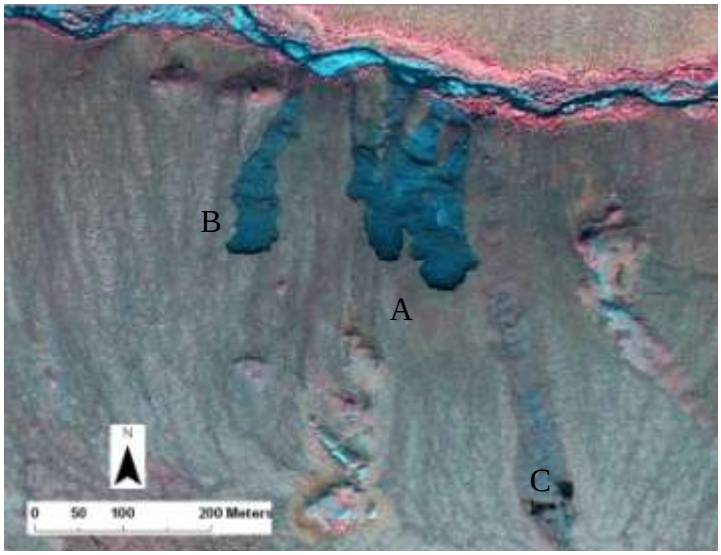

Figure 19. Setting of slumps NOAT068 (A) and NOAT069 (B) on 2008 IKONOS satellite imagery. Note the revegetated slump at (C).

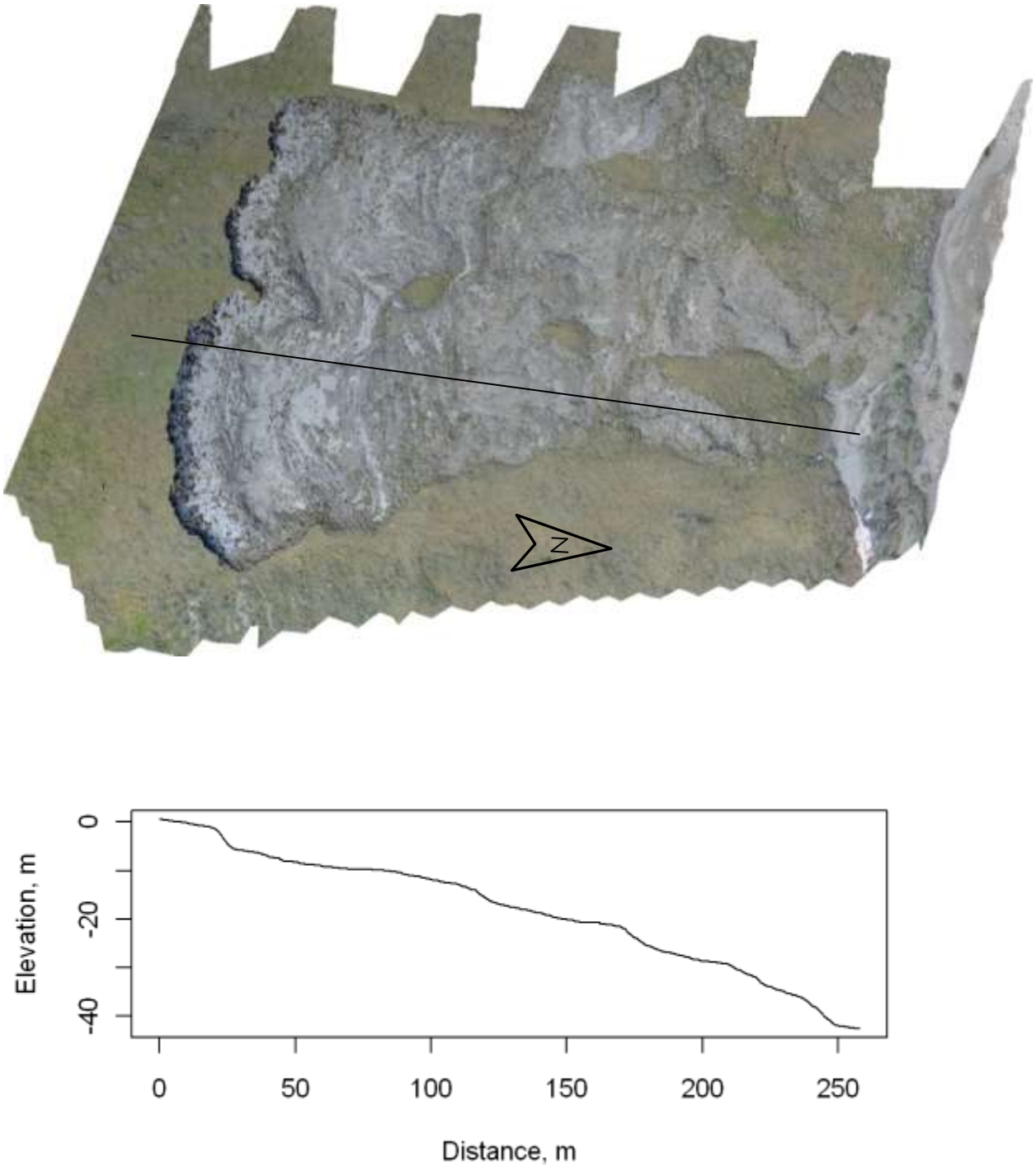

Figure 20. Orthophotograph and cross section of slump NOAT068, constructed from photography pass 2010C.

Figure 21. Main scarp of slump NOAT068 in the vicinity of the cross-section shown in Fig.20. The main scarp is about 5 m high. The upper 1.5 m is glacial till that forms a nearly vertical face. Below this is debris-rich glacial ice that forms about a 45° slope and on 22 June 2010 was thawing actively to form the adjacent zone of liquefied mud and numerous small rivulets.

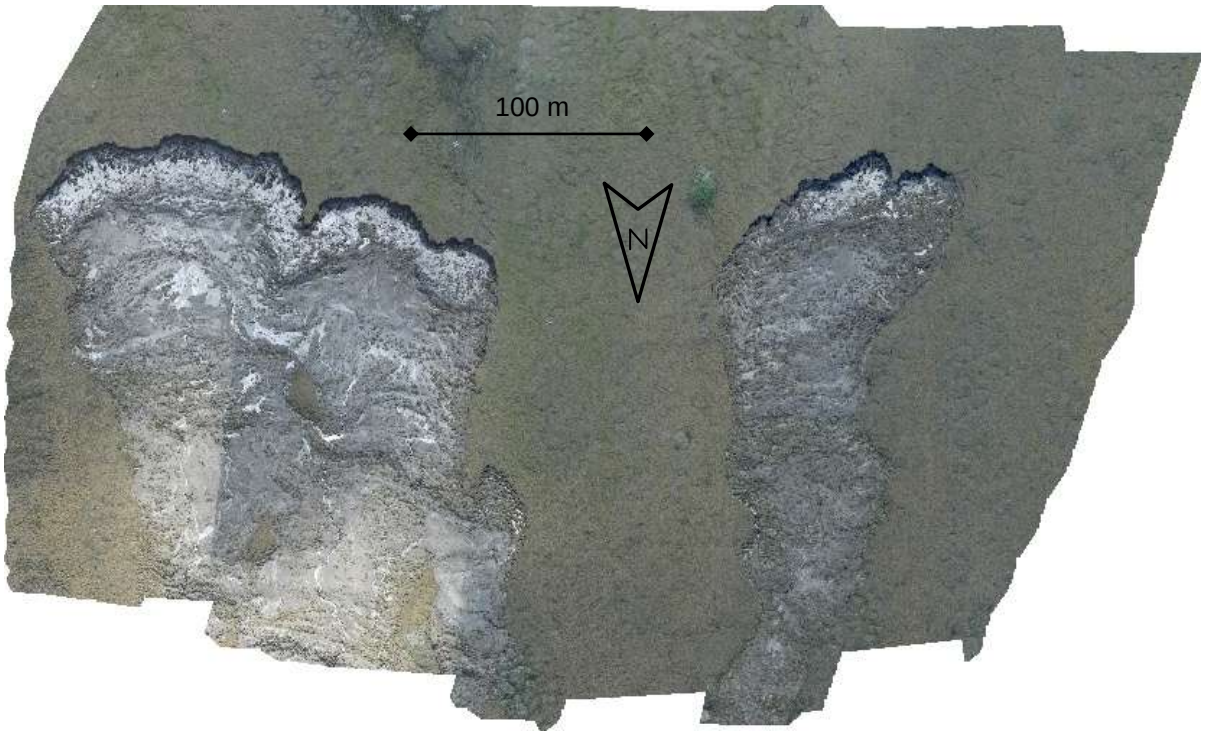

Figure 22. Orthophotograph of slumps NOAT068 (left) and NOAT069 (right), constructed from photography pass 2010B.

NOAT070

NOAT070 is a large slump with a conspicuous alluvial fan on a west-facing slope of about 10% (Figs. 23-25). The slump proper had an area of about 3.5 ha and the fan covered another 1.3 ha. The main scarp was about 4 m high and consisted of about 2 m of glacial till that formed a vertical face, over debris-rich glacial ice that formed an approximately 45° slope (Fig. 25). Below this was a zone of actively flowing, liquefied mud that became drier and firmer as one moved away from the main scarp. The slope was 5-10% in the liquefied zone, steepening in the more solid area below before declining to about 5% in the lower part of the slump floor. The slope on the alluvial fan averaged about 16%. The volume of the upper depression was about 51,500 m^3 over an area of about 2.9 ha. NOAT070 overlapped part of a slump that appeared to be weakly active in 1977 (Fig. 23); NOAT070 is currently advancing into undisturbed ground.

Table 8. Camera location and accuracy parameters for NOAT070[1].

Parameter	Mean	Minimum	Maximum
Pass 2010A			
Camera elevation, m	92	72	105
Camera angle ω, ° from vertical	63	62	65
Distance to target, m	340	246	403
Base:height ratio	0.22	0.19	0.35
Control point error in x, m	0.022		-0.040
Control point error in y, m	0.033		-0.055
Control point error in z, m	0.036		0.058
Pass 2010B			
Camera elevation, m	59	39	79
Camera angle ω, ° from vertical	62	59	65
Distance to target, m	322	266	361
Base:height ratio	0.17	0.12	0.21
Control point error in x, m	0.131		-0.252
Control point error in y, m	0.116		-0.216
Control point error in z, m	0.123		-0.189

[1]Pass 2010A - 8 photos, 6 control points; pass 2010B – 10 photos, 6 control points

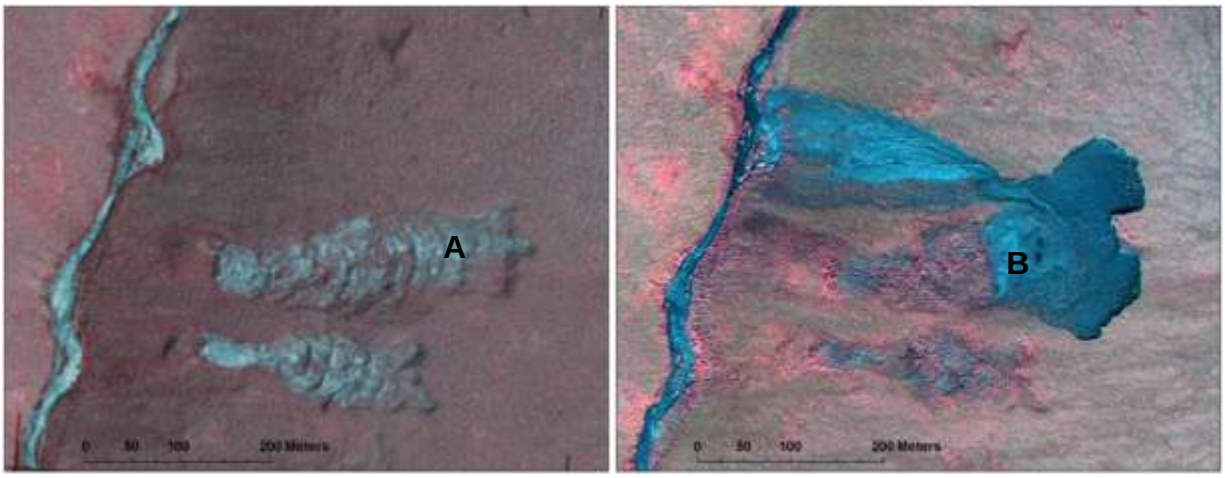

Figure 23. NOAT070 in 1977 (left, AHAP aerial photograph) in 2008 (right, IKONOS image). Two slumps were present in 1977. They appear weakly active in 1977, and this observation is confirmed by the fact that the extent of the lower slump was the same in 2008. NOAT070 (B) has reoccupied, deepened, and enlarged the upper portions of the larger old slump (A).

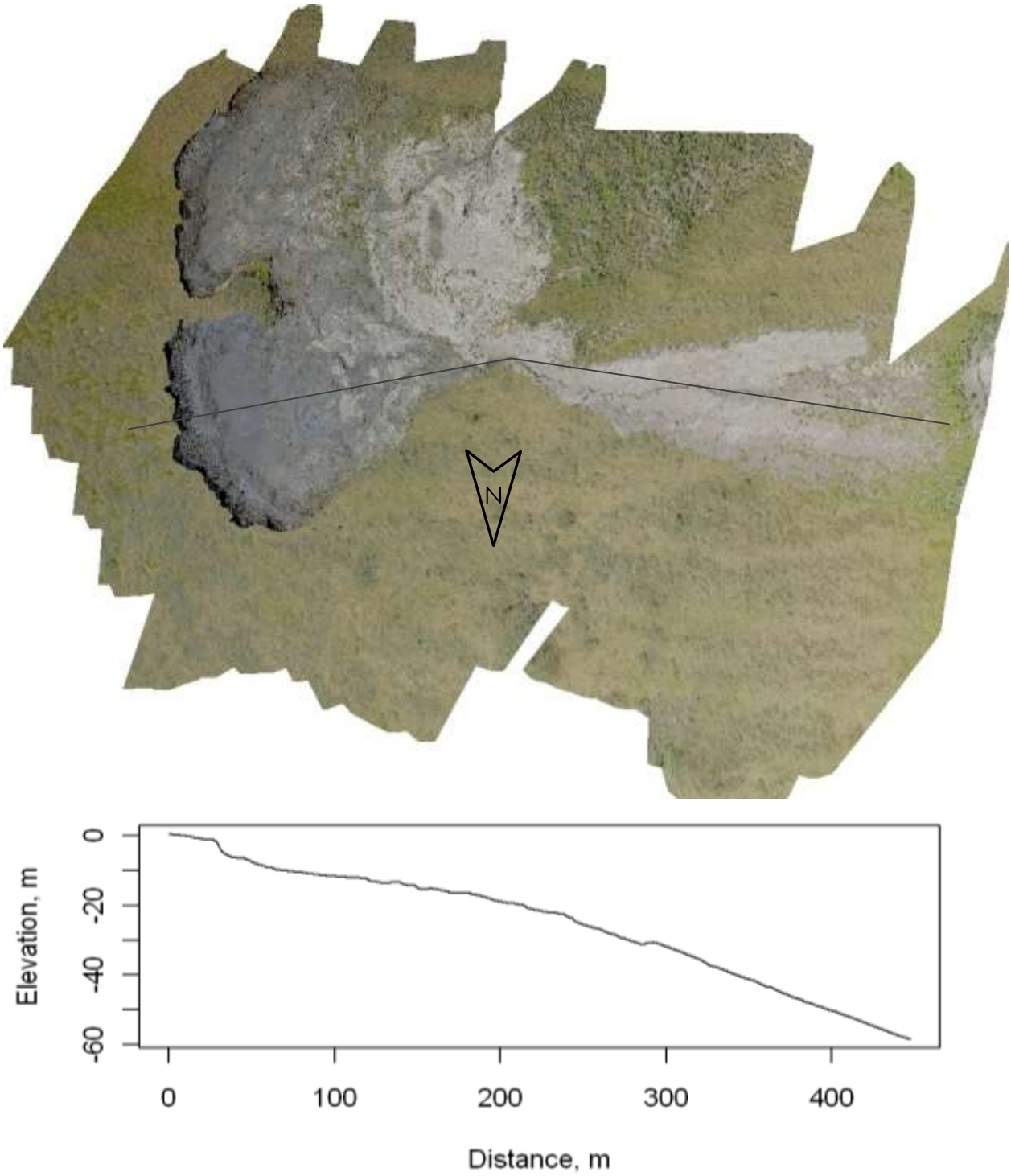

Figure 24. Slump NOAT070 orthophotograph and cross-sectional diagram. The photograph is based on pass 2010B; the cross-section is based on pass 2010B below the angle in the line and on pass 2010A (to provide better accuracy) above the angle.

Figure 25. Main scarp of slump NOAT070. The main scarp is about 4 m high and consists of about 2 m of glacial till that forms a vertical face, over debris-rich glacial ice that forms an approximately 45° slope

NOAT071, 72, and 73

These three active slumps occur together along a lake shore on Itkillik I moraine in the far eastern NOAT (Figs. 26-28). Adequate ground control was obtained for NOAT071 (Fig. 27) and photography also covered neighboring slumps (NOAT072, NOAT073; Fig. 26)

NOAT071 is a small slump with an area of about 0.75 ha on a north-facing slope of about 8%. The primary depression near the main scarp contained a volume of about 5,800 m. At the time of our visit (22 June 2010) there was no exposed ice, mud, or water near the main scarp. The main scarp was about 5 m tall at its highest point. The topographic cross section shows a series of ridges with slopes around 30°, interspersed with flatter areas with 10% slopes. Near the middle of the slump a small depression pond has formed with a steep south bank. AHAP photography from 1977 (Fig. 28) reveals some past slumping in the vicinity, though slumps were small except for the one next to NOAT072 (the slump responsible for the pond visible in Fig. 26) and they were mostly inactive in 1977. The current extents of NOAT071, -72, and -73 lack clear signs of prior slumping.

Table 9. Camera location and accuracy parameters for NOAT071[1].

Parameter	Mean	Minimum	Maximum
Pass 2010B			
Camera elevation, m	136	131	139
Camera angle ω, ° from vertical	61	59	64
Distance to target, m	262	234	272
Base:height ratio	0.19	0.15	0.25
Control point error in x, m	0.05		0.15
Control point error in y, m	0.08		0.30
Control point error in z, m	0.06		-0.21

[1]5 photos, 5 control points

Figure 26. Slumps NOAT072 (left) and NOAT073 (right). These slumps occur with NOAT071 and several revegetated slumps and smaller active slumps along 1 km of lakeshore. The pond in the upper left corner of the photo is in a basin formed by a previous RTS.

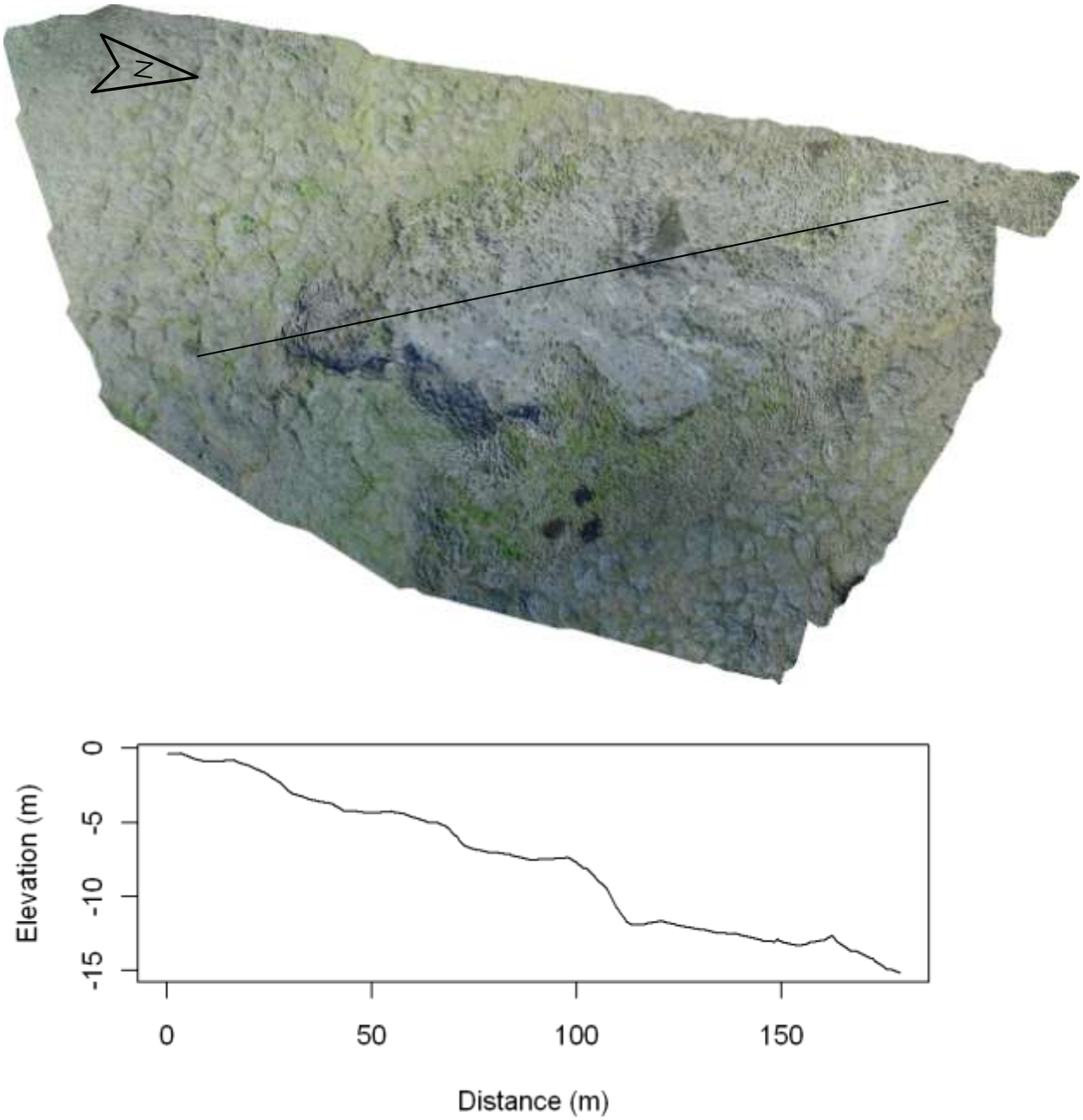

Figure 27. Orthophoto and topographic cross-section of slump NOAT071, constructed from pass 2010B.

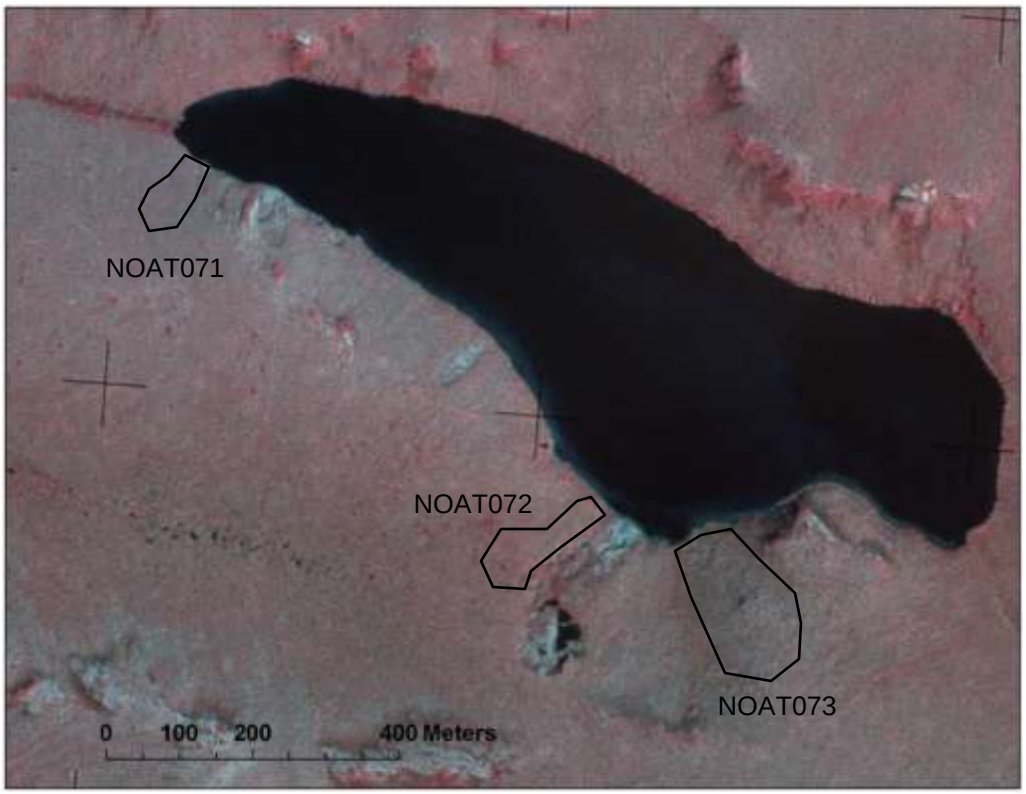

Figure 28. Slumps NOAT071, NOAT072, and NOAT073 in 1977 (AHAP aerial photography). The approximate outlines of the slump extents in 2010 are shown. Cloud-free IKONOS imagery is not available for this area.

NOAT074 and NOAT076

NOAT074 and NOAT076 are southeast- and east-facing slumps, respectively, that occur near one another on an Itkillik II glacial moraine, on a lakeshore in far eastern NOAT (Figs. 29-30). Both formed on slopes that were undisturbed in 1977, though older slumps are present in the vicinity (Fig. 30). NOAT074 and NOAT076 were photographed without ground control in 2010.

Figure 29. Retrogressive thaw slumps NOAT074 (left) and NOAT076 (right).

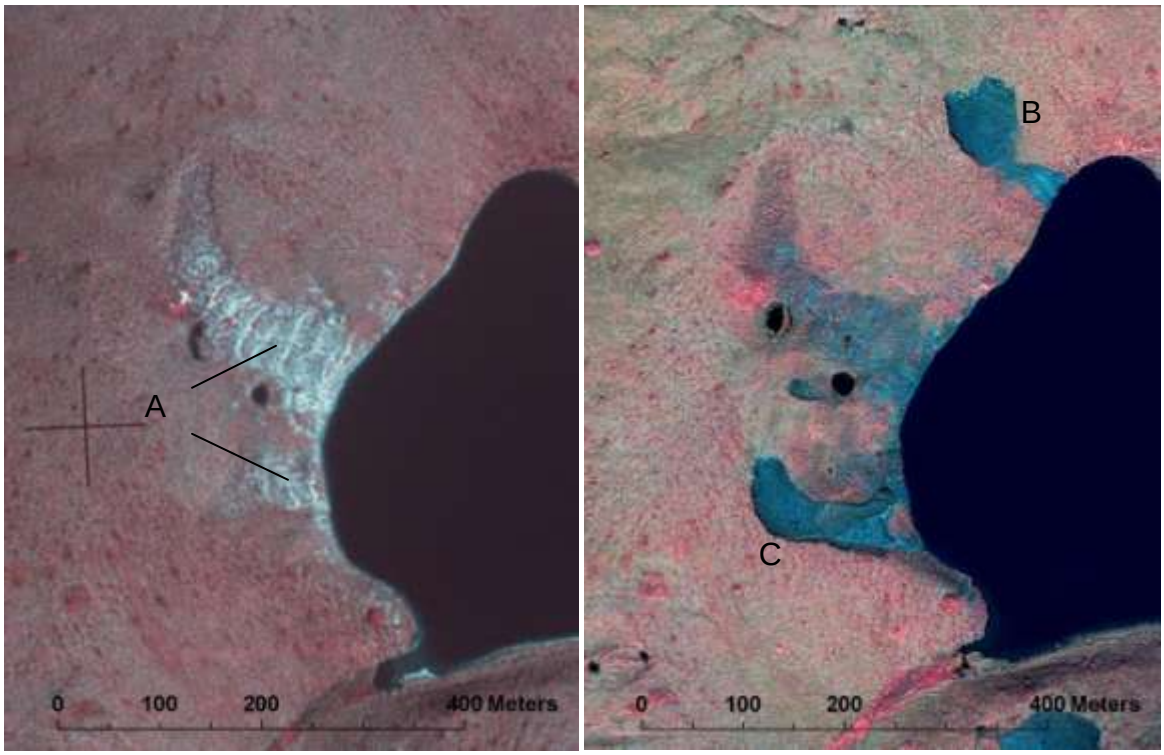

Figure 30. Retrogressive thaw slumps NOAT074 and NOAT076 in 1977 (left, AHAP photograph) and 2008 (right, IKONOS image). Slumps that appear inactive in 1977 (A) show little change since that time. NOAT074 (B) and NOAT076 (C) have developed on undisturbed slopes.

NOAT148

NOAT148 (Figs. 31-34) is a medium-sized slump on a west-northwest facing slope of about 12% on Itkillik I glacial deposits (Hamilton, 2009). The vicinity of NOAT148 had not been disturbed by slumping at the time of AHAP photography (1977). Pleistocene ice wedges and debris-rich glacial ice were exposed in the 8 m-tall main scarp (Fig. 33). The slope near the main scarp was 40-50% and gradually flattened to 5-10% (Fig. 32). A gulley ran from east to west through the lower part of the slump, leading to an alluvial fan that extended to the un-named creek at its foot. The slump had an approximate area of 1.7 ha with a volume of 26,000 m^3. Pass 2010A faces south and runs along the entire north flank of the slump. Pass 2010C details the main scarp and upper floor with high precision.

Table 10. Camera location and accuracy parameters for NOAT148[1].

Parameter	Mean	Minimum	Maximum
Pass 2010A			
Camera elevation, m	63	60	67
Camera angle ω, ° from vertical	59	57	60
Distance to target, m	206	180	253
Base:height ratio	0.16	0.10	0.24
Control point error in x, m	0.09		-0.15
Control point error in y, m	0.02		-0.04
Control point error in z, m	0.05		0.08
Pass 2010C			
Camera elevation, m	36	35	38
Camera angle ω, ° from vertical	58	56	62
Distance to target, m	118	110	133
Base:height ratio	0.15	0.21	0.29
Control point error in x, m	0.0002		0.0003
Control point error in y, m	0.0001		-0.0002
Control point error in z, m	0.0005		-0.0006

[1]Pass 2010A - 11 photos, 6 control points; pass 2010B – 11 photos, 6 control points

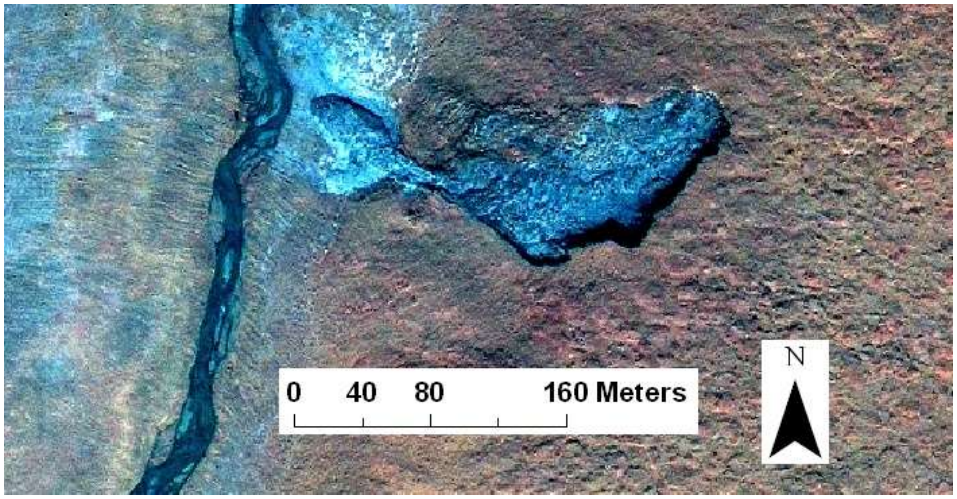

Figure 31. Overview of slump NOAT148 from 2008 IKONOS satellite imagery

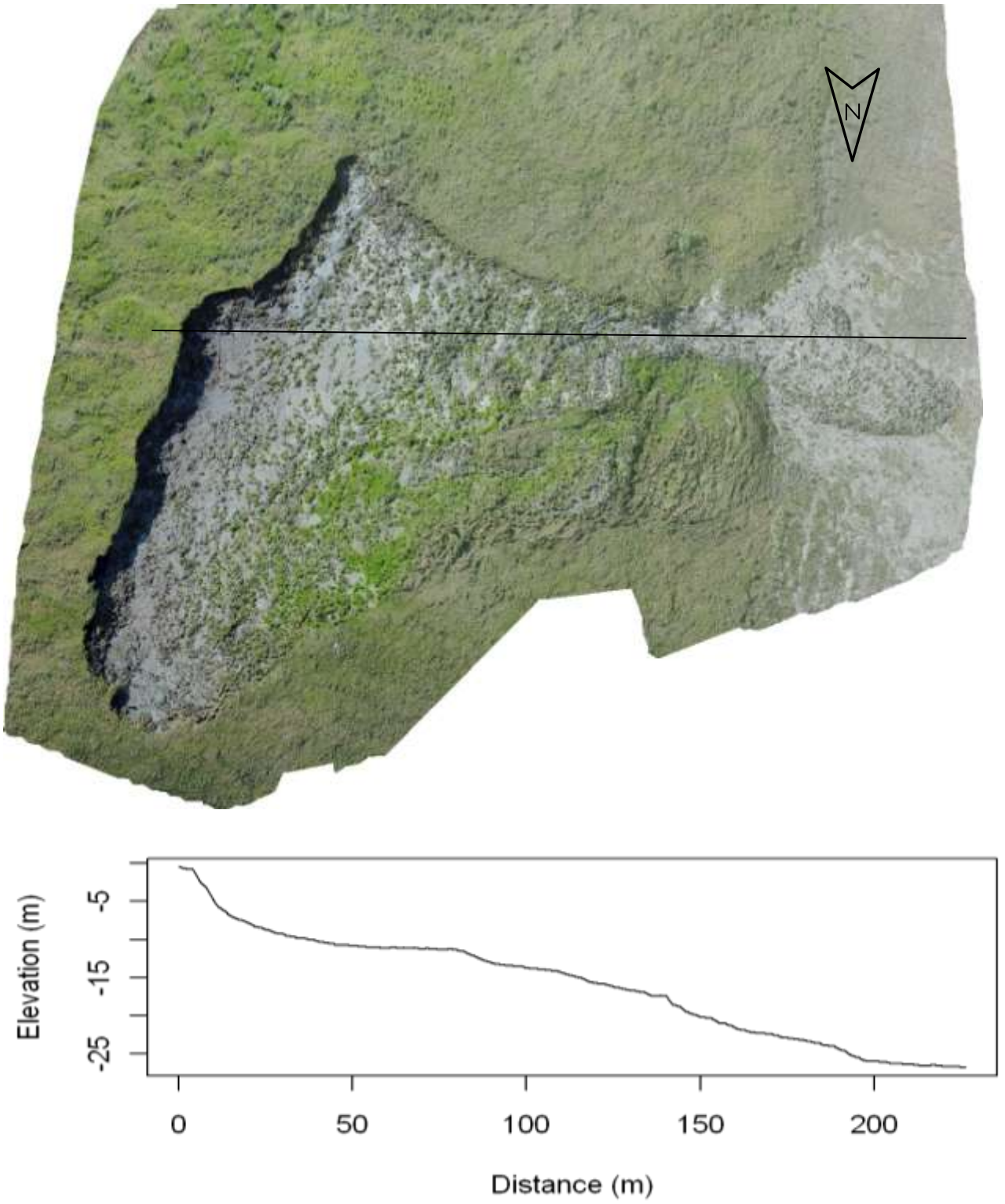

Figure 32. Orthophoto and topographic cross-sections of slump NOAT148, constructed from pass 2010A.

Figure 33. The main scarp of slump NOAT148. Large Pleistocene ice wedges (A) occur in glacial till (B).

Figure 34. Wedge and glacial ice in the main scarp of NOAT148. This exposure shows a Pleistocene ice wedge (A) cutting into debris-rich glacial ice (B). Both features are truncated above by thaw in the modern active layer (C), which is about 0.5 m thick.

NOAT151

NOAT151 is a large slump of about 4.4 ha on a slope of about 7% with east-northeast aspect (Figs. 35-37). The main scarp was 4 to 5 m high and exposed Itkillik I glacial till over debris-rich glacial ice. The slump floor was undulating with an average slope of about 8%. Part of the active escarpment of NOAT151 was advancing into an older revegetated slump (Fig. 35).

Table 11. Camera location and accuracy parameters for NOAT151[1].

Parameter	Mean	Minimum	Maximum
Pass 2010C			
Camera elevation, m	58	53	65
Camera angle ω, ° from vertical	59	57	60
Distance to target, m	215	172	274
Base:height ratio	0.18	0.17	0.20
Control point error in x, m	0.017		0.028
Control point error in y, m	0.004		-0.005
Control point error in z, m	0.007		-0.011
Pass 2010D			
Camera elevation, m	54	49	59
Camera angle ω, ° from vertical	58	53	60
Distance to target, m	226	166	265
Base:height ratio	0.016	0.011	0.029
Control point error in x, m	0.003		-0.003
Control point error in y, m	0.002		0.004
Control point error in z, m	0.001		0.002

[1]Pass 2010C - 15 photos, 4 control points; Pass 2010D – 18 photos, 5 control points

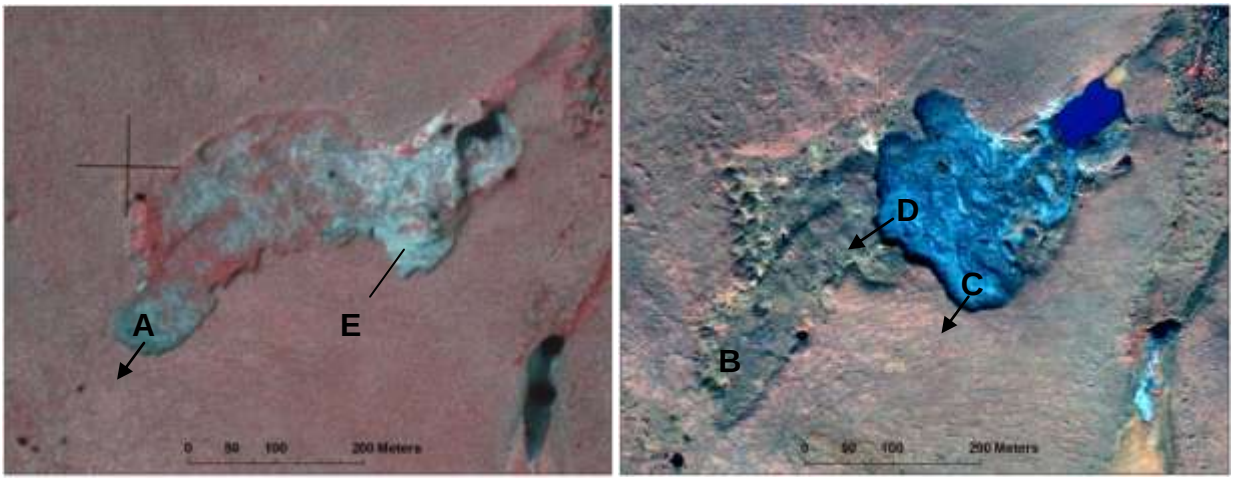

Figure 35. NOAT151 in 1977 (left, AHAP aerial photograph) and 2008 (right, IKONOS image). The uppermost of the 1977 slump (A) was active and moved further uphill (in the direction of the arrow) before stabilizing (B). NOAT151 is advancing to the left both into undisturbed ground (C) and by deepening the older slump (D). Part of the current slump appears to have been active in 1977 (E)

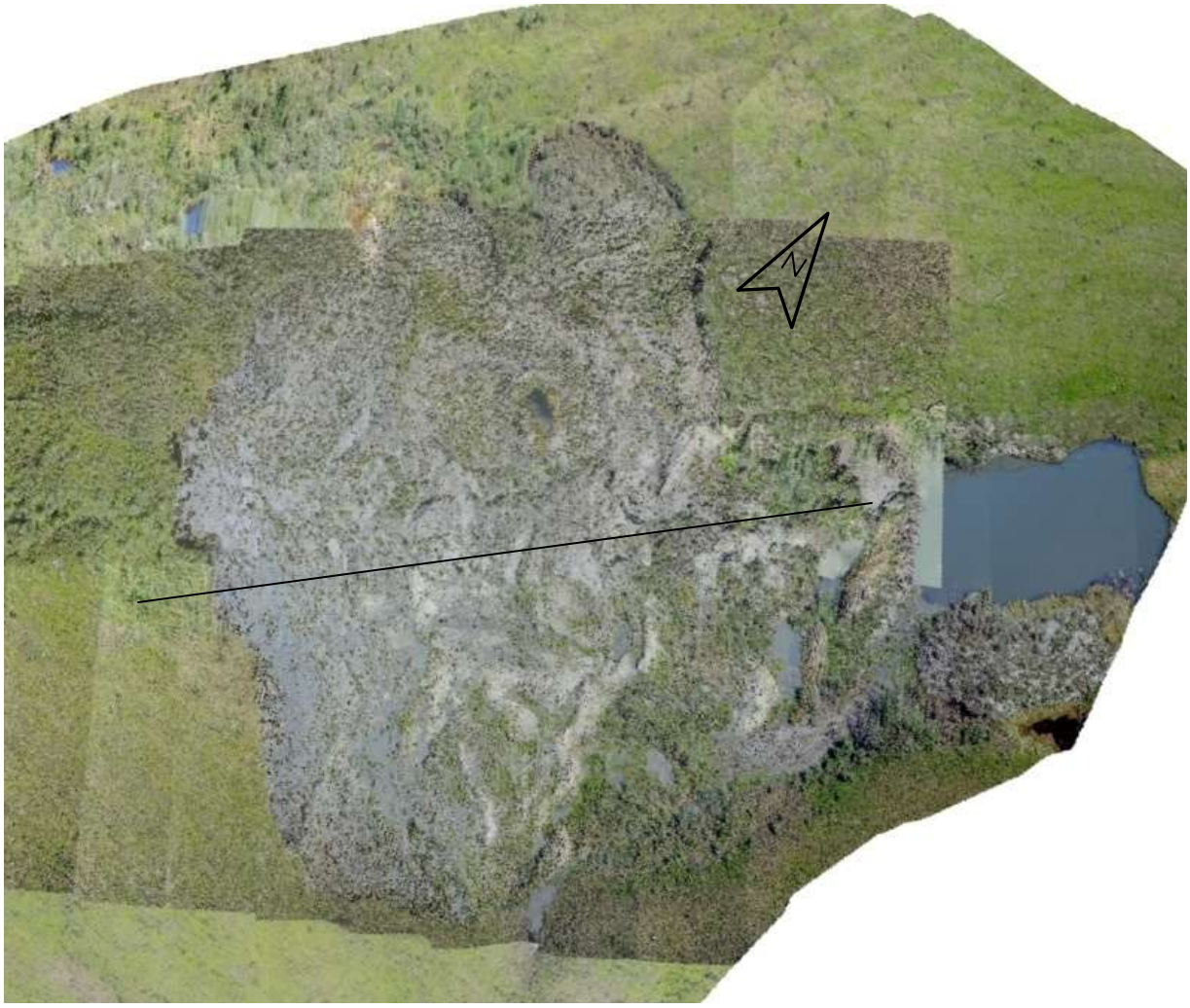

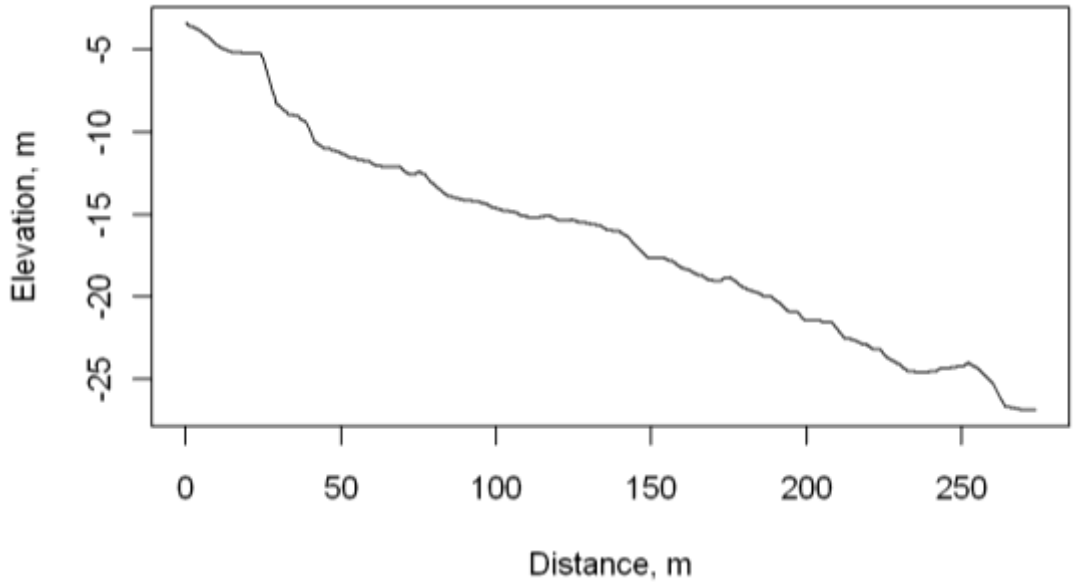

Figure 36. Orthophotograph and topographic cross-section of slump NOAT151, constructed by merging passes 2010C and 2010D.

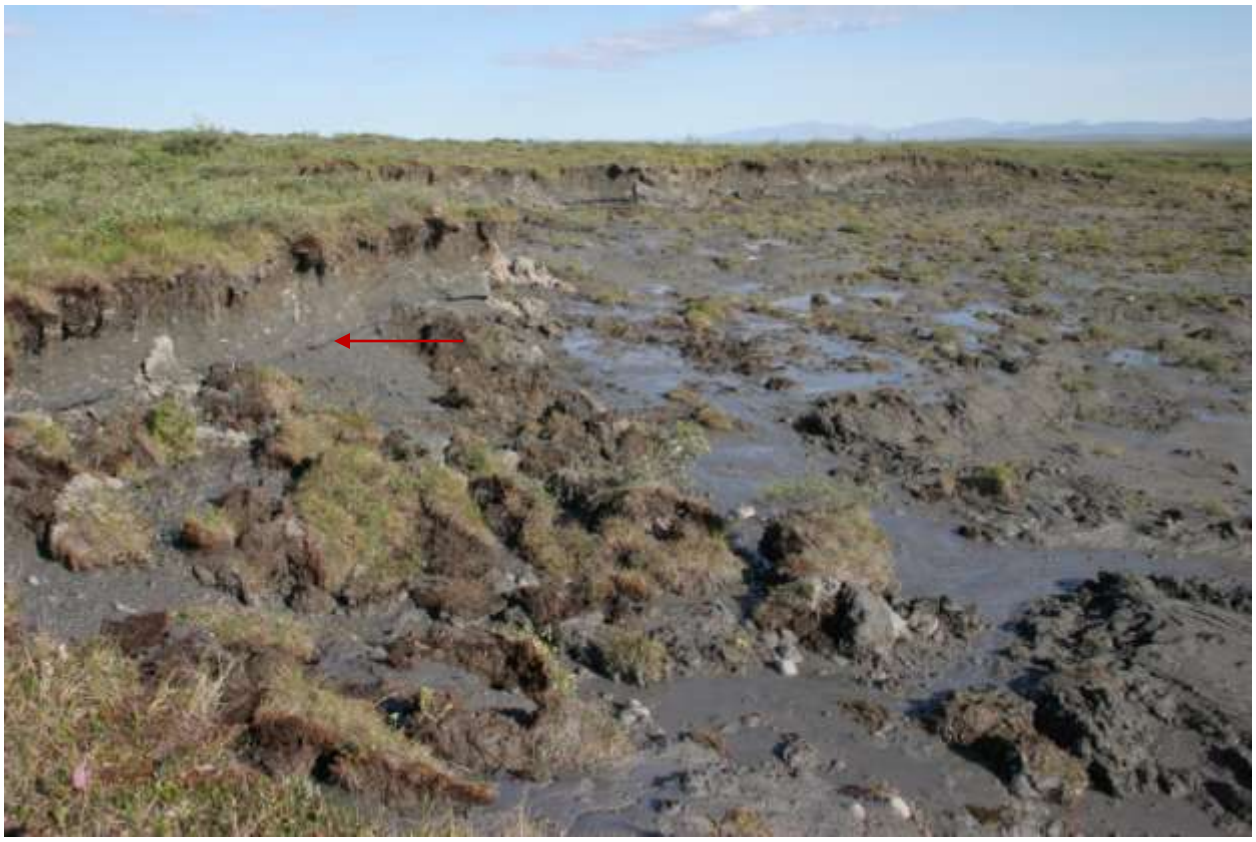

Figure 37. Main scarp of NOAT151. The total height, including the vertical upper part and slope with vegetated slump blocks, is 4 to 5 m. The distinct horizontal line visible about 2 m below the surface (marked with an arrow) is the boundary between glacial till above and debris-rich glacial ice below. The shiny areas are water-saturated, liquefied mud.

NOAT159 and NOAT160

NOAT159 and NOAT160 occur in close proximity on a lakeshore in Itkillik II moraine (Hamilton, 2009) in far eastern NOAT (Figs. 38-39). They have a generally easterly aspect. Both slumps reached the lake, and the sediment supplied to the lake gave it a milky color. There were two inactive slumps that directly flank NOAT159. Slumps NOAT159, NOAT160, and the inactive slumps near the former have developed since 1977 on undisturbed slopes (Fig. 39). The larger inactive slump expanded about 150 m and partly revegetated in between 1977 and 2008 (Fig. 39), a scarp migration rate of well over 5 m per year. NOAT 159 and NOAT160 were photographed without ground control in 2010.

Figure 38. Slumps NOAT159 (left) and NOAT160 (right)

Figure 39. Slumps NOAT159 and NOAT160 in 1977 (left, AHAP photograph) and 2008 (right, IKONOS image). NOAT159 (A) and NOAT160 (B) formed on a slope that was undisturbed in 1977. The partially revegetated slumps that flank NOAT159 were also not present in 1977.

NOAT161

NOAT161 is medium-sized, low-relief slump on a slope of about 11% with west-northwest aspect, located in a slump-rich Itkillik II moraine area (Hamilton, 2009) in far eastern NOAT (Figs. 40-42). It is on the shore of a small lake, and it had a small alluvial fan that reaches the lake, though it had no running water at the time of our visit (25 June 2010). The slump proper had an area of about 1.4 ha, with the fan covering an additional 0.3 ha. The upper depression of about 1.1 ha had a volume of about 8,200 m^3. The main scarp was about 2 m high at its highest point and exposed a continuous layer of debris-rich glacial ice about 1.5 m below the surface. This ice was actively melting to produce liquefied mud that flowed away from main scarp. As the mud flowed downslope it de-watered and gained strength. Pressure on this more solid mud from the liquid material uphill caused it to buckle upward and form a low ridge parallel to the main scarp and about 5 m from it. This same process was probably responsible for the series of similar ridges visible further down the slump, at distances of about 70, 90, 135, and 175 m on the cross-section. Above each of these minor escarpments the slope of the slump floor declined to near zero, producing an overall slope on the floor of about 10%. Examination of AHAP aerial photography from 1977 shows that the present site of NOAT161 was undisturbed at that time.

Table 12. Camera location and accuracy parameters for NOAT161[1].

Parameter	Mean	Minimum	Maximum
Pass 2010A			
Camera elevation, m	132	107	148
Camera angle ω, ° from vertical	53	51	57
Distance to target, m	305	285	323
Base:height ratio	0.14	0.12	.018
Control point error in x, m	0.013		.0.25
Control point error in y, m	0.030		-0.044
Control point error in z, m	0.018		-0.027

[1]7 photos, 6 control points

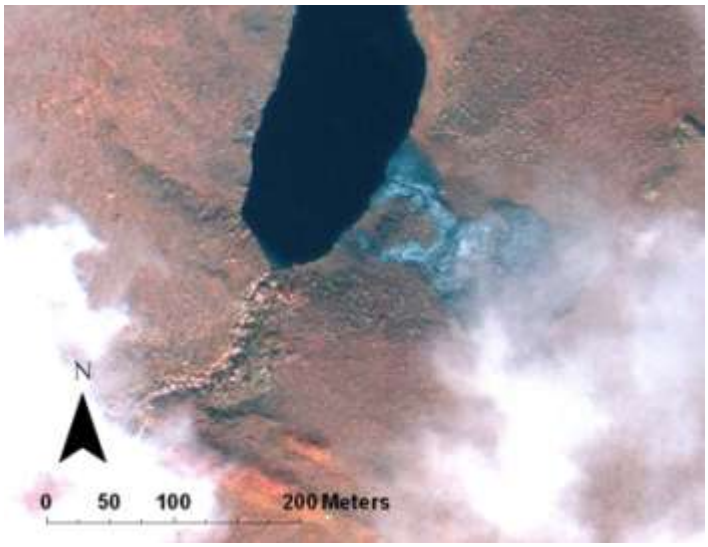

Figure 40. NOAT161 overview, on 2008 IKONOS image partially obscured by clouds.

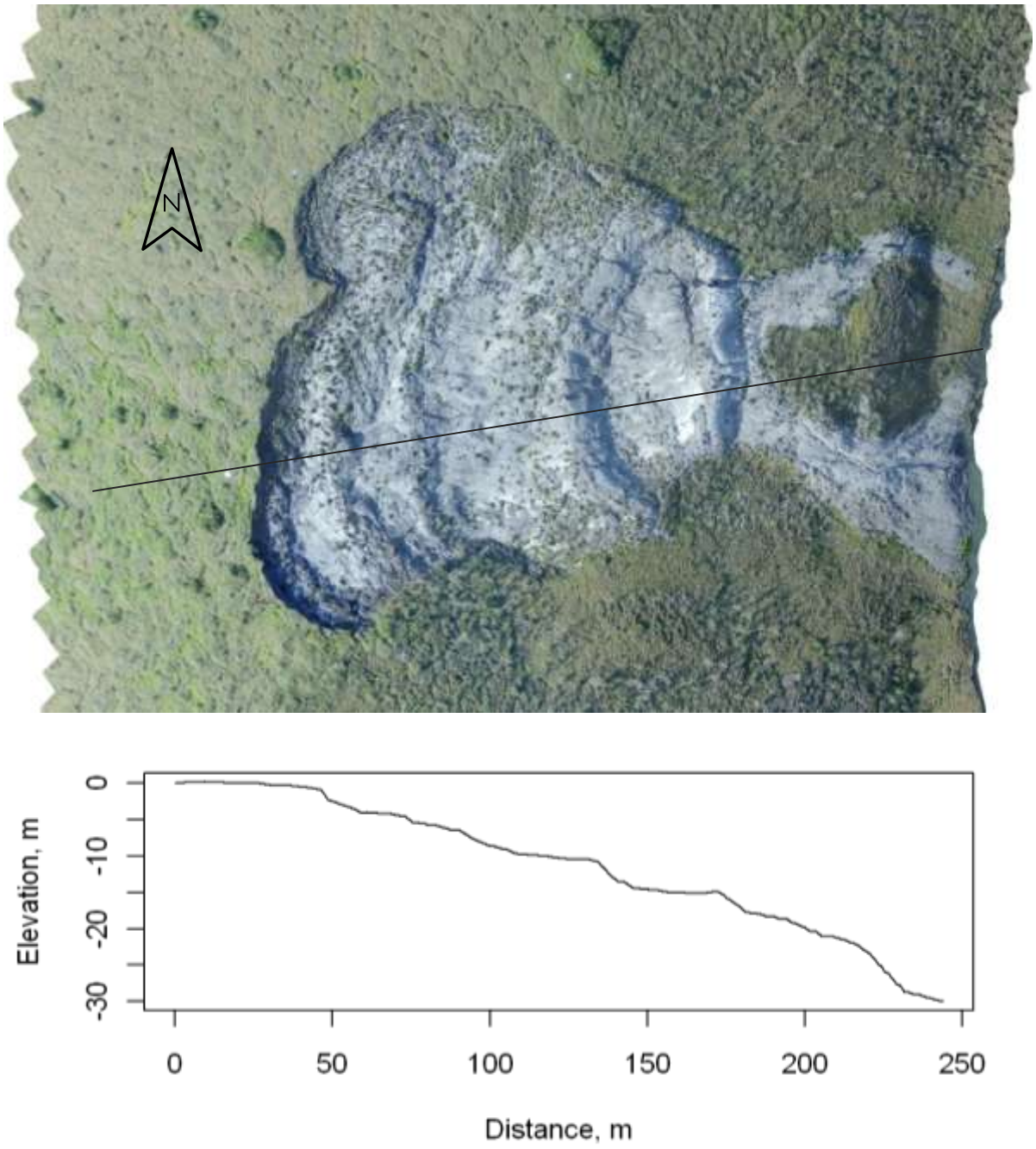

Figure 41. Orthophotograph and topographic cross-section of slump NOAT161 on 25 June 2010, based on photography pass 2010A.

Figure 42. Close-up of main scarp of slump NOAT161. The scarp exposes about 1.5 m of glacial till (A), over glacial ice (B) that is melting to produce a liquefied mud zone (C).

NOAT172

NOAT172 is a slump with area of about 1.2 ha and main scarp about 10 m tall, on a 14% slope with northwest aspect (Figs. 43-47). In the upper 0.76 ha of the slump, where it is a distinct depression with bounding walls, the volume change due to subsidence has been about 22,000 m^3. The main scarp exposed glacial till containing large Pleistocene ice wedges. Below the main scarp was a zone of liquefied mud that de-watered and became firmer as it moved away from the main scarp. The upper 25 m of the slump floor sloped at 20 to 30%; below this zone it became quite flat, firm, and stable though still sparsely vegetated and subject to surface erosion by running water. A small snowbank persisting from the previous winter was present at the foot of the main scarp on 21 June 2010. Examination of AHAP aerial photography showed the present site of NOAT172 was undisturbed in 1979.

Pass 2010B runs up the left flank of the slump and provides coverage of the main slump area. Pass 2010C faces the main scarp and covers the upper half of the slump including an additional lobe and partially revegetated region on the left flank; it also provides a better view of the scarp along the left flank than pass 2010B. The orthophotograph and cross-sections were derived from a merged TIN from the two passes.

Table 13. Camera location and accuracy parameters for NOAT172[1].

Parameter	Mean	Minimum	Maximum
Pass 2010B			
Camera elevation, m	61	56	67
Camera angle ω, ° from vertical	62	60	66
Distance to target, m	192	171	216
Base:height ratio	0.26	0.22	0.30
Control point error in x, m	0.007		0.011
Control point error in y, m	0.013		0.025
Control point error in z, m	0.013		0.021
Pass 2010C			
Camera elevation, m	75	65	85
Camera angle ω, ° from vertical	61	60	63
Distance to target, m	302	298	310
Base:height ratio	0.29	0.22	0.35
Control point error in x, m	0.028		0.041
Control point error in y, m	0.007		0.013
Control point error in z, m	0.013		0.019

[1]Pass 2010B - 7 photos, 6 control points; 4 photos, 6 control points

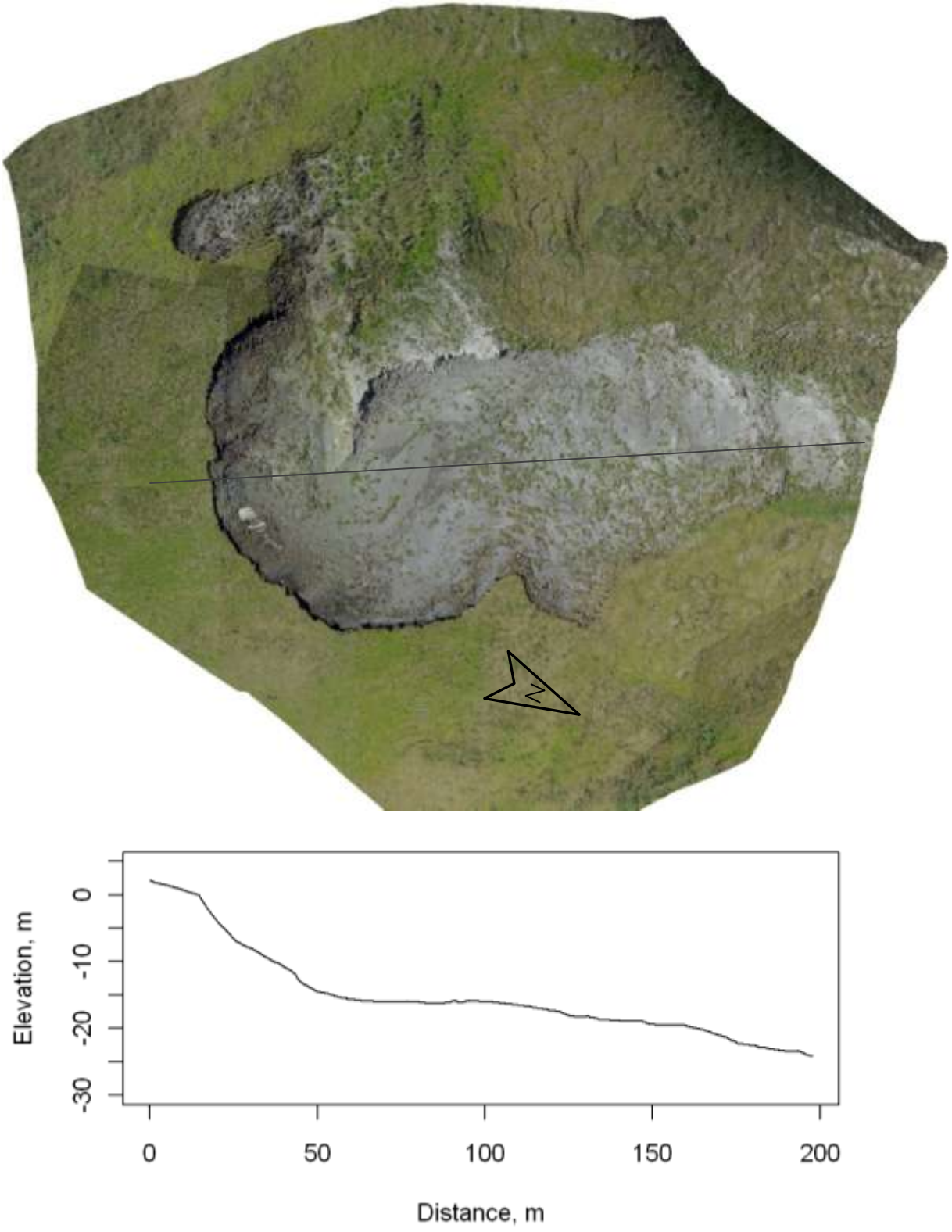

Figure 43. Orthophotograph and topographic cross section of slump NOAT172, based on a merge of pass 2010B (lower half of the photo) and 2010C (upper half of photo).

Figure 44. Synthetic 3D view of main scarp region of slump NOAT172. Red lines give locations of the complete topographic cross-section (right line; Fig. 43) and the close-up cross section of the steep main scarp region (left line; Fig. 45). An on-the-ground close-up near the left cross-section is in Fig. 46.

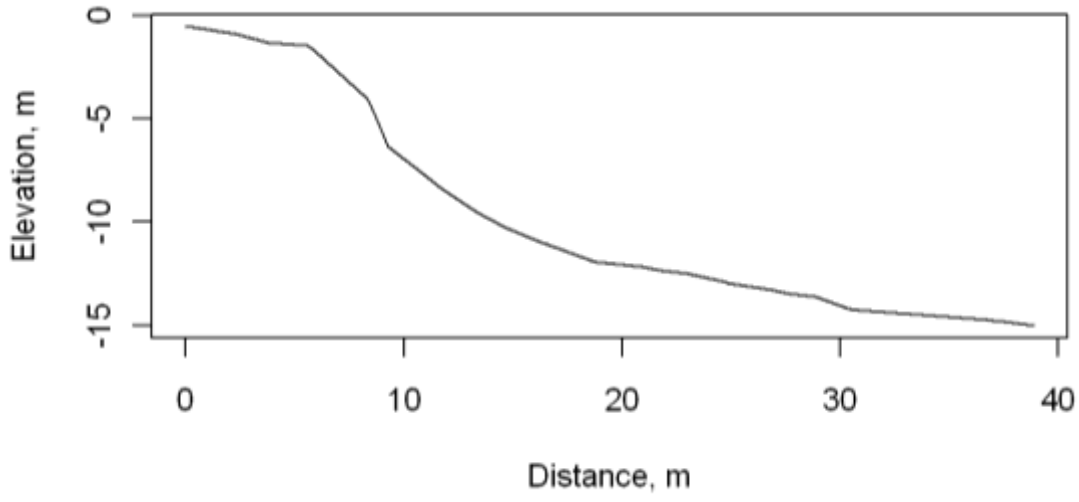

Figure 45. Topographic cross-section of the main scarp region of NOAT172, outlined in Fig. 44. Based on pass 2010B.

Figure 46. Main scarp region of slump NOAT172 on 21 June 2010. Shiny near-vertical faces on the left and in the center are large Pleistocene ice wedges.

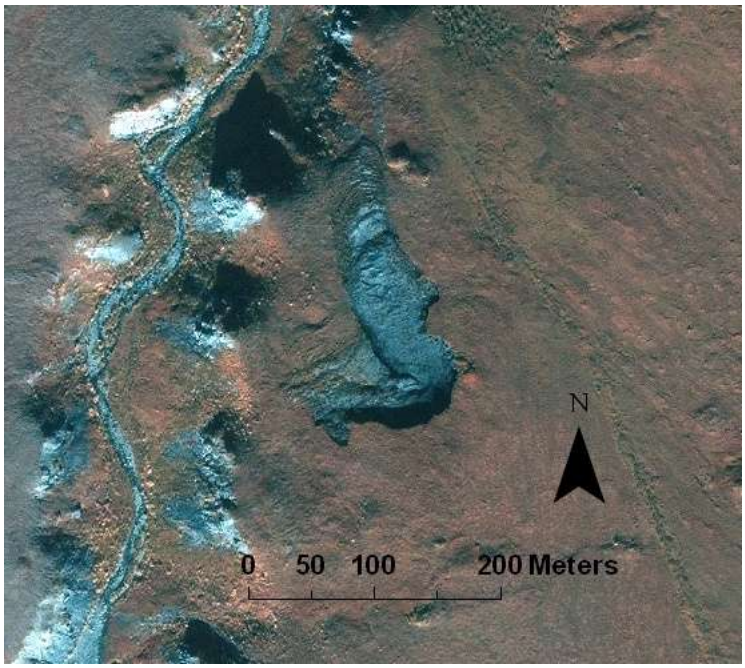

Figure 47. NOAT172 overview on 2008 IKONOS image.

NOAT225

NOAT225 is a medium-sized slump with area of about 1.2 ha, on a west-facing slope of about 11% (Fig. 48-49). It had a long (0.5 km) alluvial fan that ended on the slope about 1 km from Kavachurak Creek. The main scarp was about 5 m high but did not expose any ground ice on 22 June 2010. The upper part of the slump formed a depression with area of about 0.68 ha and volume of 11,320 m^3. The floor consisted of a series of flats with slopes of less than 10% and step-like steeper bands oriented perpendicular to the slope; the overall slope of the floor was about 10%. Examination of AHAP aerial photography showed the present site of NOAT225 was undisturbed in 1979.

Table 14. Camera location and accuracy parameters for NOAT225[1].

Parameter	Mean	Minimum	Maximum
Pass 2010A			
Camera elevation, m	103	99	109
Camera angle ω, ° from vertical	68	68	66
Distance to target, m	458	433	470
Base:height ratio	0.2	0.19	0.22
Control point error in x, m	0.006		0.008
Control point error in y, m	0.002		0.002
Control point error in z, m	0.015		0.017

[1]4 photos, 4 control points

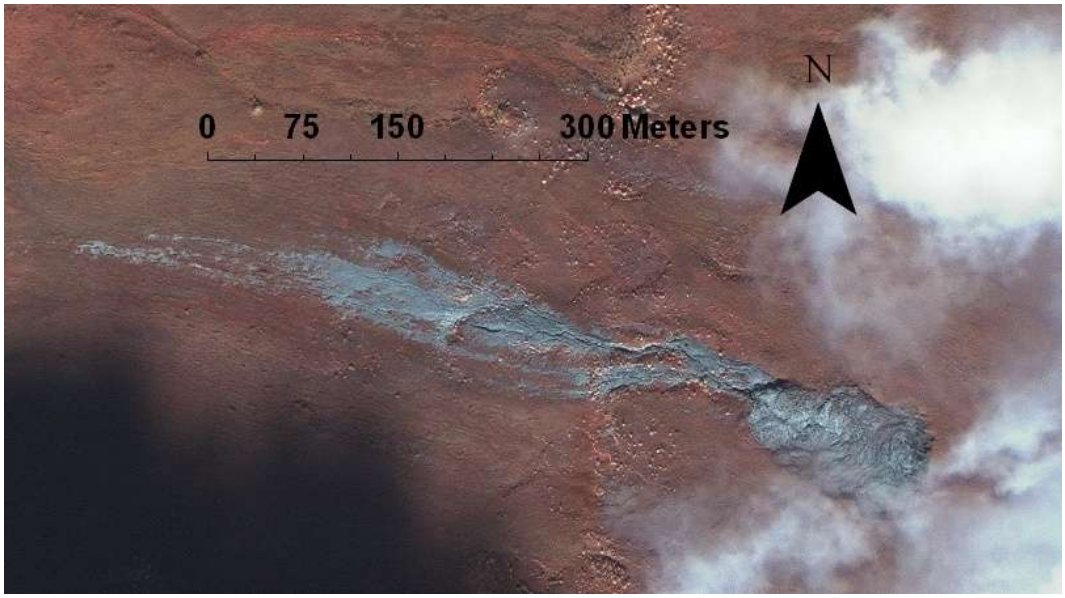

Figure 48. Overview of slump NOAT225 from 2008 IKONOS imagery.

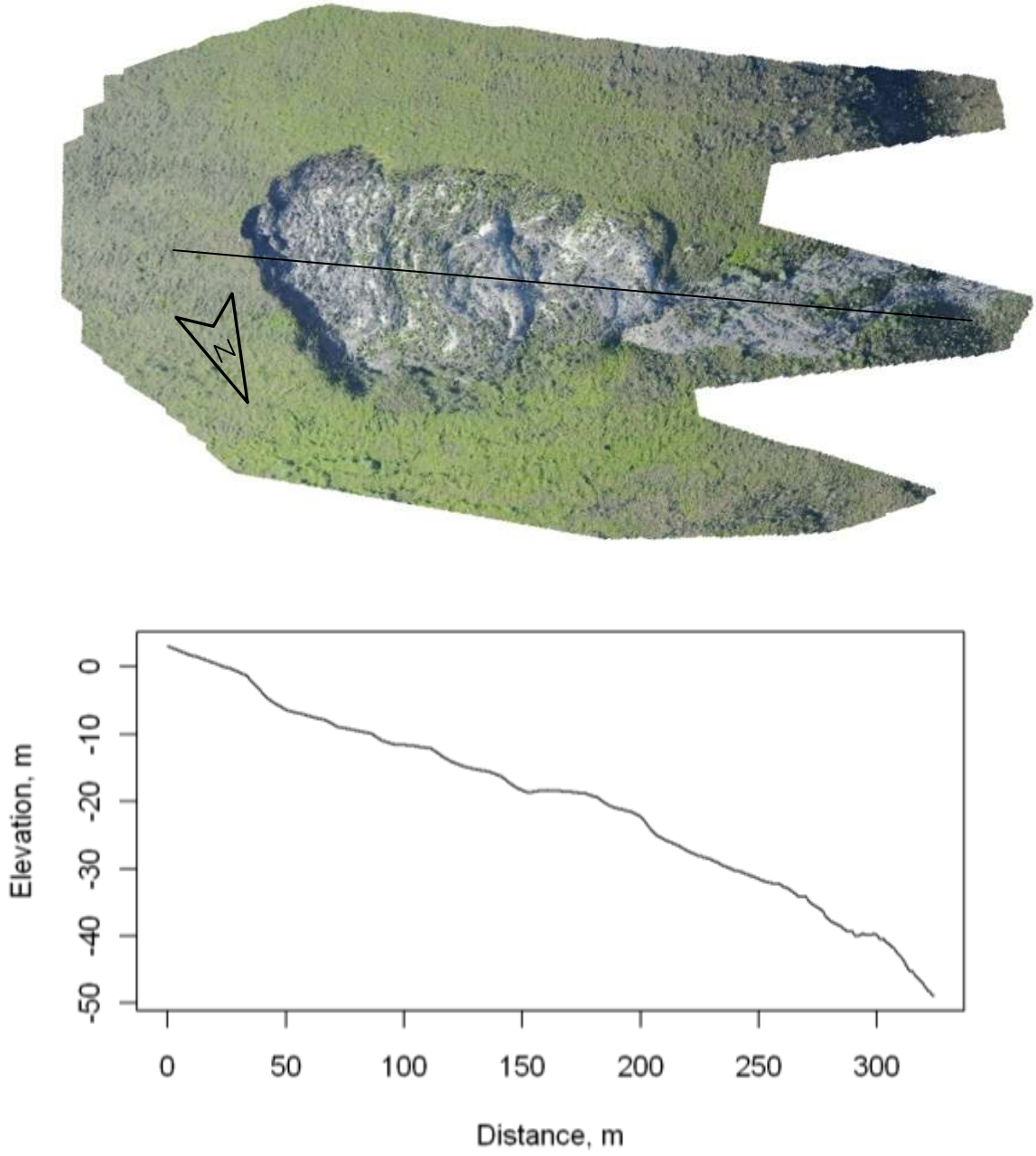

Figure 49. Orthophoto and topographic cross-section of slump NOAT225, based on pass 2010A.

NOAT237 and NOAT238

NOAT237 and NOAT238 form a large, east-southeast facing slump complex on the shore of a small lake (Figs. 50-51). Both have retreated a long distance from their lakeshore origin and the lower, older portions have substantially revegetated, although the lake is still cloudy from their sediment input. Minor slumping was occurring in the area in 1980, but the current slumps NOAT237 and NOAT238 have formed since then (Fig. 51). These slumps were photographed without ground control in 2010.

Figure 50. Slumps NOAT238 (left) and NOAT237 (right). These photos were taken along a single flight line and overlap slightly.

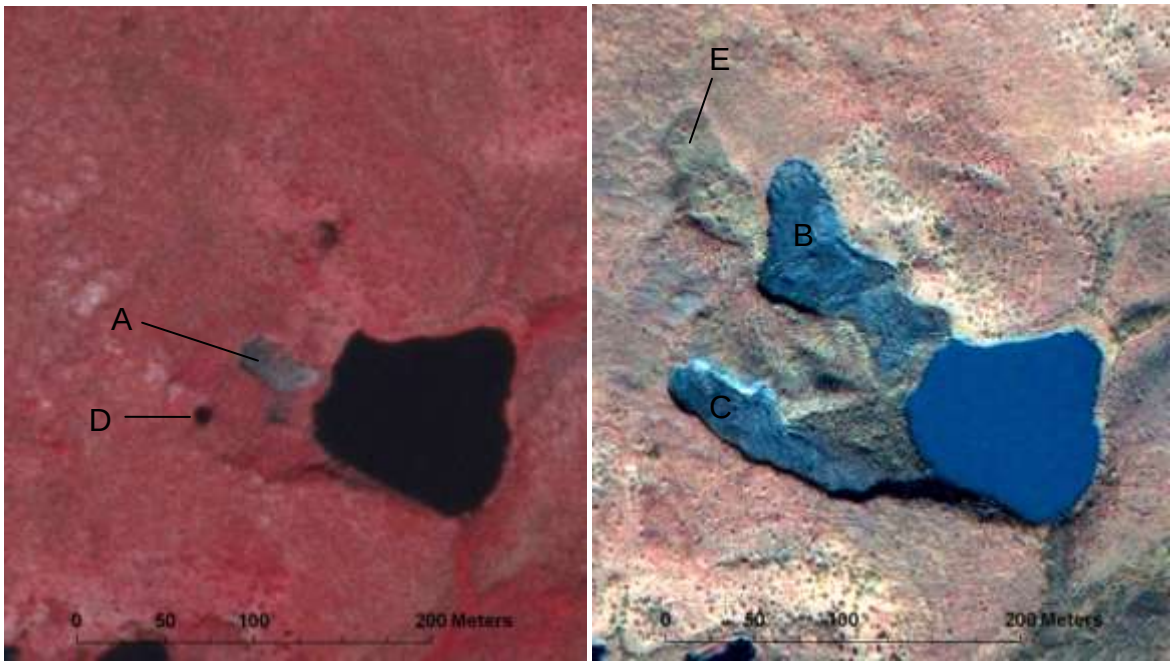

Figure 51. Slumps NOAT237 and NOAT238 in 1980 (left, AHAP photography) and 2008 (right, IKONOS imagery). A small slump present in 1980 (A) and located between today's active slumps has revegetated. NOAT237 (B) and NOAT238 (C) have formed on areas that were mostly undisturbed in 1980, though the small pond at (D) in 1980 was probably of thermokarst origin. The slump at (E) formed and revegetated between 1980 and 2008.

NOAT247 and NOAT248

NOAT247 and NOAT248 (Figs. 52-54) are adjacent slumps on an east-northeast facing slope of about 12% on the shore of a small lake, in Itkillik I glacial deposits (Hamilton, 2009). The area of NOAT247 (the southern slump) was 0.75 ha, and NOAT248 (the northern one) was 0.62 ha. They had rather high escarpments, nearly 5 m at the highest point on NOAT247, but no ice was exposed on 23 June 2010, and the slump floors were almost entirely dry and hard, even near the main scarp. The floors of the slumps averaged about 10%, steepening near the lake shore. The distinct basin in the upper part of NOAT247 with an area of about 0.73 ha had a volume of about 11,100 m^3, while on the smaller NOAT248 the basin of 0.47 ha had a volume of about 6,070 m^3. Both slumps have re-occupied the area of previous slumps that had revegetated prior to 1980 (Fig. 52).

Table 15. Camera location and accuracy parameters for NOAT247 and 248[1].

Parameter	Mean	Minimum	Maximum
Pass 2010A			
Camera elevation, m	82	75	93
Camera angle ω, ° from vertical	60	59	61
Distance to target, m	222	188	262
Base:height ratio	0.19	0.17	0.22
Control point error in x, m	0.028		0.038
Control point error in y, m	0.078		-0.132
Control point error in z, m	0.038		-0.059

[1]9 photos, 6 control points

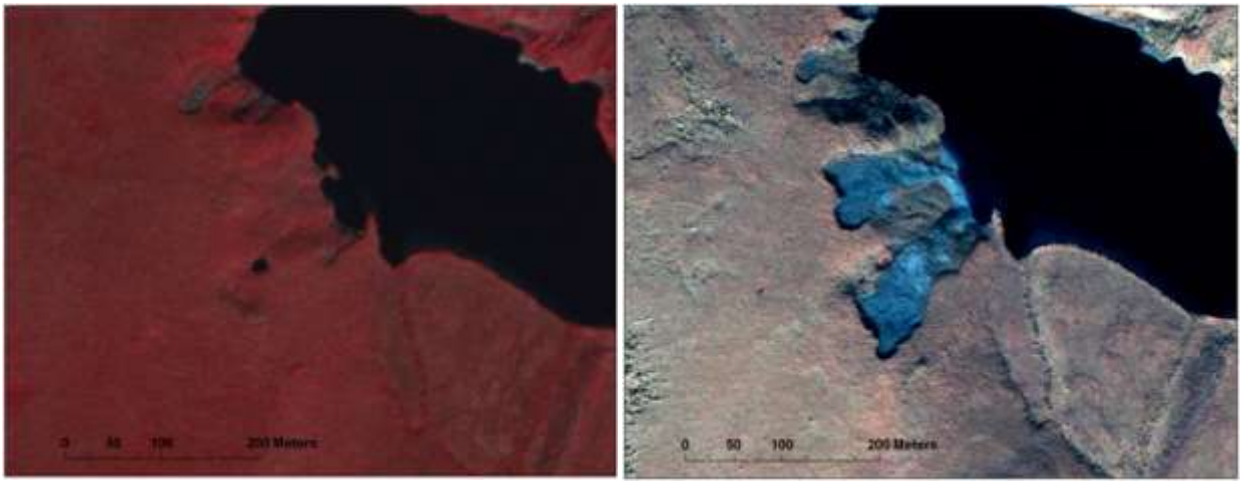

Figure 52. NOAT247 and NOAT248 in 2008 (left, IKONOS imagery) and 1980 (right, AHAP aerial photography). The slumps have reoccupied and enlarged upon previous slumps that had stabilized in 1980.

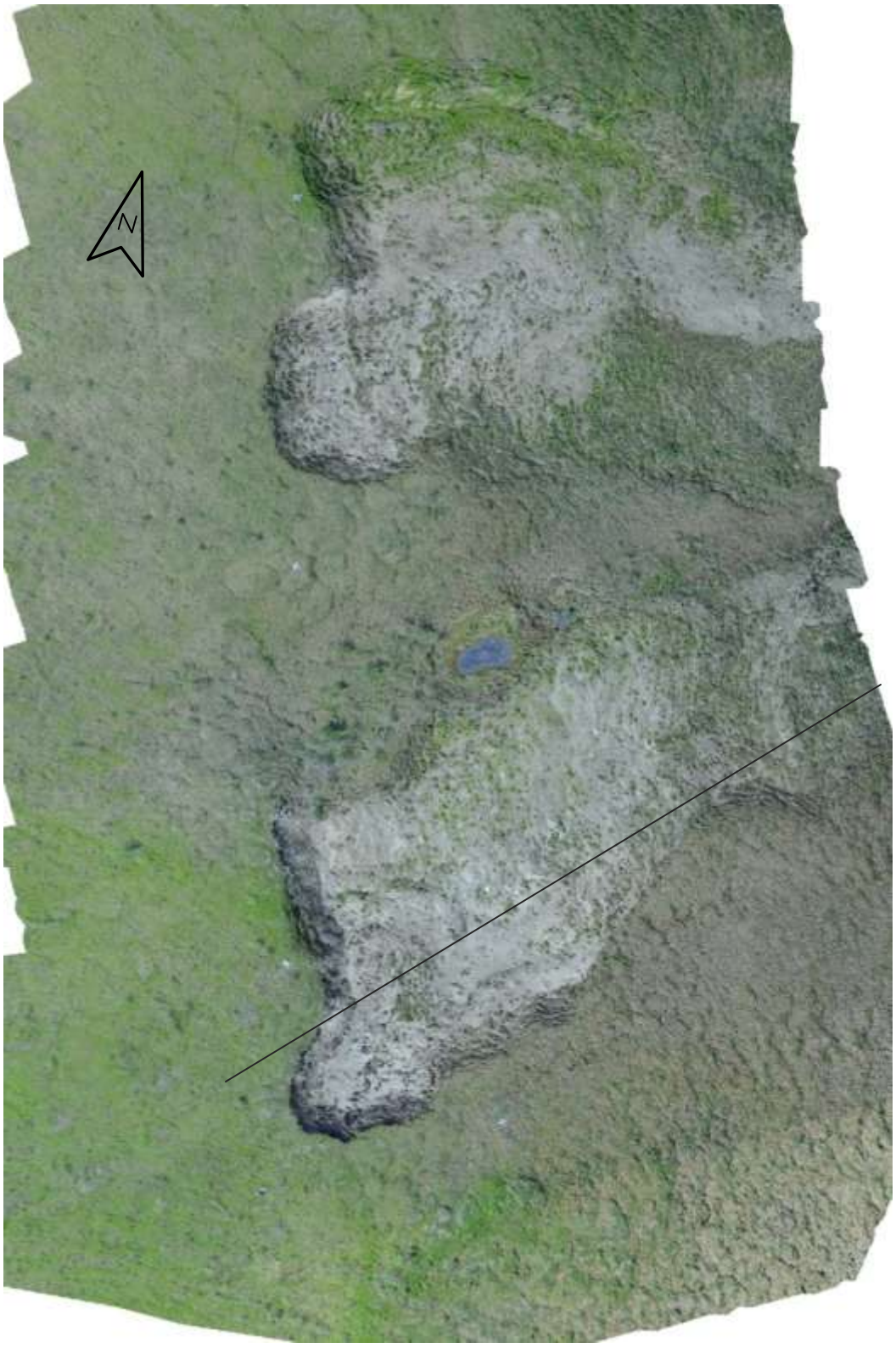

Figure 53a. Orthophotograph of slump NOAT247 (lower) and NOAT248 (upper) based on pass 2010A. Scale is provided by the topographic cross-section (Fig. 53b), along the line on Fig. 53a.

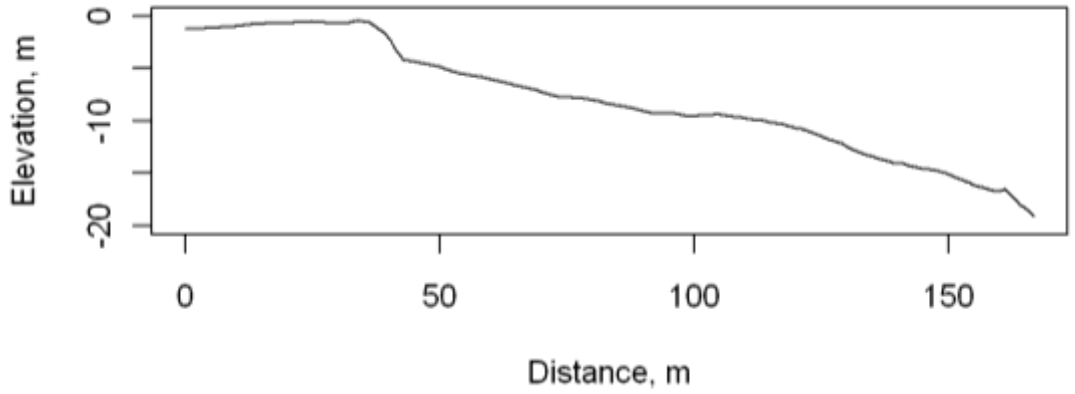

Figure 53b. Topographic cross-section of slump NOAT247. The cross-section alignment is given on Fig. 53a.

Figure 54. Oblique aerial photograph of main scarp region of slump NOAT247. The photograph is centered near the cross-section line shown on Fig. 53. An aerial target (1.5 m across) is visible above the main scarp near the photo center.

Discussion

The retrogressive thaw slumps in this study have morphologies and settings similar to what has been described in the past (Burn and Lewkowicz, 1990; Lantuit and Pollard, 2005, 2008; Kokelj et al., 2009; Lacelle et al., 2010). In several cases the slumps active today were advancing into ground that slumped previously and revegetated. Multiple episodes of slumping across the same ground has been described previously at other locations (Lantuit and Pollard, 2008; Kokelj et al, 2009; Lacelle et al. 2010) and this pattern indicates that slumping episodes can stabilize by development of sufficient overburden of sediment on the ice, without melting all of the ice.

The zone of liquefied mud present below the main scarp results from melting of ground ice, which releases more water than can be absorbed in the pore space of the sediment that is also released by thaw. Pieces of intact sod floating in the liquefied zone, and similar sod islands visible on the slump floors, survived the fall from the scarp and could serve as propagule sources for revegetation of the slump. The mud on the slump floor became firmer with distance from the main scarp as it de-watered. The firmer material below the liquefied zone can act as a dam, restricting downhill flow of liquefied sediment. In some cases this dam material was deformed into a low ridge parallel to the main scarp, with fractures indicating upward buckling due to compression by the flowing mud above. The slump floor profiles frequently displayed a series of flats and gentle steps that appear to be former liquefied zones and associated sediment dams. At the moment we are unsure what time interval these bands represent. The slump floors beyond the narrow current liquefied zone and dam were dry, firm, and showed no fresh fractures or deformation, though rivulets and small gullies indicating surface water erosion were common. Apparently viscous flow of mud is usually restricted to the main scarp vicinity and further sediment transport is by surface water. Surface water erosion and transport can be considerable, as shown by the alluvial fans present below some of the slumps.

Retrogressive thaw slumps in our study occur exclusively on glacial till deposits, and glacial ice was present in many main scarp exposures. This suggests that in our study area, glacial deposits may be used to predict where the ice masses that lead to retrogressive thaw slumping are likely to be present. The glacial origin of massive ground ice has been refuted by Mackay and Dallimore (1992) in northwestern Canada, and consequently scientists there have searched for non-glacial explanations for the ice in RTS (Lacelle et al., 2004). However, more recent work in northwestern Canada by Murton et al. (2005) has supported a glacial origin for massive tabular ice bodies under till, similar to what we observed in NOAT. The conditions that make our study area ideal for RTS are 1) widespread glacial till deposits with sufficiently fine grain size to allow liquefaction by super-saturation with water, and 2) continuous permafrost that has preserved glacial ice for many thousands of years since glaciation.

The area of the slumps is not strongly related to main scarp height and age of the geological material, at least in our non-random sample of slumps (Table 2). However, the height of the main scarps and hence volume of subsidence is clearly greater on older surfaces with large ice wedges. Obviously, if two slumps of similar width have equal rates of scarp migration but different scarp heights, the one with the higher scarp will have a higher rate of volume loss, but future monitoring will be needed to understand the relationship between ground ice types, geological setting, and the rate of scarp migration and slump growth.

The fact that only one of the study slumps was on a south-facing slope suggests a pattern that should be tested in the future using the set of all RTS from our inventory of NOAT and GAAR (see the Introduction). All the slumps are in the zone of continuous permafrost, and thus south-facing slopes have suitable conditions for the existence of ground ice at the present.

From examination of the c. 1980 aerial photography we know that slumping was occurring at that time in the vicinity of today's slumps. The revegetated outlines of the 1980s-era slumps are visible today, and they generally became revegetated with little or no growth beyond the 1980 outline. Also, today's active slumps are not (with two exceptions, NOAT039 and NOAT151) the result of continued migration of scarps active in 1980. In other words, the slumps that were active in 1980 stabilized soon thereafter; today's slumps initiated in different (though sometimes nearby) areas and grew to their present size since 1980. The main scarps of the study slumps have migrated between 100 and 300 m in 30 years or less, indicating minimum migration rates of 3 m to 10 m per year. The aim of our future monitoring will be refine these rate estimates and better understand the processes which lead to slump to stabilization or continued growth. We are also interested in whether climatic change will affect slumping activity in the future. Comparisons of slump growth rates from this study with weather data should be useful in this regard. In a related study (Swanson, 2010, and in-progress studies in NOAT and GAAR), we are mapping the area occupied by retrogressive thaw slumps and active-layer detachments across all of ARCN on recent satellite imagery, as a baseline for comparisons to the past and future.

Literature Cited

Balser, A. W. W. B. Bowden, J. B. Jones, M. N. Gooseff, D. M. Sanzone, A. Bouchier, A. Allen, 2007. Thermokarst distribution in the Noatak Basin, Alaska: increased frequency and correlations with local and regional landscape variables. American Geophysical Union, Fall Meeting 2007, abstract #C32A-08.

Beltran, L., D. M. Cruden, E. Krauter, G. Lefèvre, G.I. Ter-Stepanian, and Z. Zhouyuan. 1993. Multilingual landslide glossary. The International Geotechnical Societies' UNESCO Working Party for World Landslide Inventory. Bi-Tech Publishers, Richmond, B.C. Canada. 50 pp.

Bowden, W. B., M. N. Gooseff, A. Balser, A. Green, B. J. Peterson, J. Bradford. 2008. Sediment and nutrient delivery from thermokarst features in the foothills of the North Slope, Alaska: Potential impacts on headwater stream ecosystems. Journal of Geophysical Research, Vol. 113, G02026, 12 pp

Burn, C. R. and A. G. Lewkowicz. 1990. Retrogressive thaw slumps. Canadian landform examples – 17. The Canadian Geographer 34(3):273–276.

Crosby, B. T., 2009, Progressive Growth, Modulated Supply: How coupling and decoupling between an enormous retrogressive thaw slump and its depositional fan impacts sediment delivery to the Selawik River, Northwest Alaska, Eos Trans. AGU, XX(XX), Fall Meeting Supplement, Abstract U41C-0043.

Czudek, T. and J. Demek. 1970. Thermokarst in Siberia and its influence on the development of lowland relief. Quaternary Research 1:103–120.

Hamilton, T.D. 1980. Surficial geologic map of the Killik River Quadrangle, Alaska: U.S. Geological Survey Miscellaneous Field Studies 1234, scale 1:250,000.

Hamilton, T. D. 2009. Guide to surficial geology and river-bluff exposures, Noatak National Preserve, northwestern Alaska. U.S. Geological Survey Scientific Investigations Report 2008-5125.

Jorgenson, M. T. and T. E. Osterkamp. 2005. Response of boreal ecosystems to varying modes of permafrost degradation. Canadian Journal of Forest Research 35:2100-2111.

Jorgenson, M. T., Y. L. Shur, and E. R. Pullman. 2006. Abrupt increase in permafrost degradation in Alaska. Geophysical Research Letters 33:L02503.

Jorgenson, T., K. Yoshikawa, , M. Kanevskiy, Y. Shur, V. Romanovsky, S. Marchenko, G. Grosse, J. Brown, and B. Jones. 2008. Permafrost characteristics of Alaska. Proceedings of the Ninth International Conference on Permafrost. University of Alaska Fairbanks, Institute of Northern Engineering.

Kokelj, S. V., R. E. Jenkins, D. Milburn, C. R. Burn, and N. Snow. 2005. The influence of thermokarst disturbance on the water quality of small upland lakes, Mackenzie Delta region, Northwest Territories, Canada. Permafrost and Periglacial Processes 16:343-353.

Kokelj, S. V., T. C. Lantz, J. Kanigan, S. L. Smith, and R. Coutts. 2009. Origin and polycyclic behavior of tundra thaw slumps, Mackenzie Delta region, Northwest Territories, Canada. Permafrost and Periglacial Processes 20:173-184.

Lacelle, D., J. Bjornson, B. Lauriol, I. D. Clark, and Y. Troutet. 2004. Segregated-intrusive ice of subglacial meltwater origin in retrogressive thaw flow headwalls, Richardson Mountains, NWT, Canada. Quaternary Science Reviews 23(5-6):681-696.

Lacelle, D., J. Bjornson, and B. Lauriol. 2010. Climatic and geomorphic factors affecting contemporary (1950-2004) activity of retrogressive thaw slumps on the Aklavik Plateau, Richardson Mountains, NWT, Canada. Permafrost and Periglacial Processes 21:1-15.

Lantuit, H. and W. H. Pollard. 2005. Temporal stereo-photogrammetric analysis of retrogressive thaw slumps on Herschel Island, Yukon Territory. Natural Hazards and Earth Systems Sciences 5:413-423

Lantuit, H. and W. H. Pollard. 2008. Fifty years of coastal erosion and retrogressive thaw slump activity on Herschel Island, southern Beaufort Sea, Yukon Territory, Canada. Geomorphology 95:84-102.

Lantz, T. C. and S. V. Kokelj. 2008. Increasing rates of retrogressive thaw slump activity in the Mackenzie Delta region, N.W.T., Canada. Geophysical Research Letters 35, L06502, 5 pp.

Lawler, J. P., S. D. Miller, D. M. Sanzone, J. Ver Hoef, and S. B. Young. 2009. Arctic network vital signs monitoring plan. Natural Resource Report NPS/ARCN/NRR-2009/088. U.S. Department of the Interior, National Park Service, Natural Resource Program Center, Ft. Collins, Colorado.

Mackay, J. R. and S. R. Dallimore. 1992. Massive ice of the Tuktoyaktuk area, western Arctic coast, Canada. Canadian Journal of Earth Sciences 29(6):1235-1249.

Murton, J. B., C. A. Whiteman, R. I. Waller, W. H. Pollard, I. D. Clarke, S. R. Dallimore. 2005. Basal ice facies and supraglacial melt-out till of the Laurentide Ice Sheet, Tuktoyaktuk Coastlands, western Arctic Canada. Quaternary Science Reviews 24:681-708.

Swanson, D. K. 2010. Mapping of erosion features related to thaw of permafrost in Bering Land Bridge National Preserve, Cape Krusenstern National Monument, and Kobuk Valley National Park. Natural Resource Data Series NPS/ARCN/NRDS—2010/122. National Park Service, Fort Collins, Colorado.

Western Regional Climate Center (WRCC). 2010. Western U.S. Climate Historical Summaries. http://www.wrcc.dri.edu/Climsum.html (accessed 15 October 2010).